Intermolecular Dissociation Energies of Dispersively Bound Complexes of Aromatics with Noble Gases and Nitrogen

Richard Knochenmuss, Rajeev K. Sinha,* and Samuel Leutwyler†

Department of Chemistry and Biochemistry,

University of Bern, Freiestrasse 3, CH-3012 Bern, Switzerland

(Dated: February 22, 2018)

Abstract

We measured accurate intermolecular dissociation energies D_0 of the supersonic jet-cooled complexes of 1-naphthol (1NpOH) with the noble gases Ne, Ar, Kr, Xe and with N_2, using the stimulated-emission pumping resonant two-photon ionization (SEP-R2PI) method. The ground-state values $D_0(S_0)$ for the 1NpOH·S complexes with S= Ar, Kr, Xe and N_2 were bracketed to within ± 3.5 %; they are 5.67 ± 0.05 kJ/mol for S=Ar, 7.34 ± 0.07 kJ/mol for S=Kr, 10.8 ± 0.28 kJ/mol for S=Xe, 6.67 ± 0.08 kJ/mol for isomer 1 of the 1NpOH·N_2 complex and 6.62 ± 0.22 kJ/mol for the corresponding isomer 2. For S=Ne the upper limit is $D_0 < 3.36$ kJ/mol. The dissociation energies increase by $1 - 5\%$ upon $S_0 \rightarrow S_1$ excitation of the complexes. Three dispersion-corrected density functional theory (DFT-D) methods (B97-D3, B3LYP-D3 and ωB97X-D) predict that the most stable form of these complexes involves dispersive binding to the naphthalene "face". A more weakly bound Edge isomer is predicted in which the S moiety is H-bonded to the OH group of 1NpOH; however, no Edge isomers were observed experimentally. The B97-D3 calculated dissociation energies $D_0(S_0)$ of the Face complexes with Ar, Kr and N_2 agree with the experimental values within $< 5\%$, but the $D_0(S_0)$ for Xe is 12% too low. The B3LYP-D3 and ωB97X-D calculated $D_0(S_0)$ values exhibit larger deviations to both larger and smaller dissociation energies. For comparison to 1-naphthol, we calculated the $D_0(S_0)$ of the carbazole complexes with S=Ne, Ar, Kr, Xe and N_2 using the same DFT-D methods. The respective experimental values have been previously determined to within < 2 %. Again, the B97-D3 results are in the best overall agreement with experiment.

Keywords: dispersive interactions, non-classical hydrogen bond, intermolecular binding energies, laser spectroscopy

I. INTRODUCTION

Intermolecular London dispersion forces are weak when viewed on a per-atom basis and act at longer range (3-10 Å) than chemical bonds, but they are ubiquitous and are always attractive.[1,2] They play a major role in the formation of molecular solids, liquids and solutions and are important for understanding their structures , lattice energies, phonon spectra, melting points, enthalpies and many other properties.[3–12] Synthetic chemists have recognized that dispersion interactions can be employed as control elements for reactivity and catalysis, in particular, for larger molecules, for which the dispersion energy contributions accumulate.[11]

However, the accurate treatment of intermolecular dispersion interactions between polyatomic molecules has proven to be remarkably challenging. Major advances have been achieved by the introduction of dispersion-corrected density functionals, which were tailored to include long-range correlation effects.[12–17] However, the parametrization of the widely-used dispersion corrections employed in DFT-D methods is mainly based on calculations.[12,15–17] Furthermore, several databases on which the DFT-D methods have been tested are themselves based on calculations; thus, the well-known S22 database for intermolecular interactions is purely computational.[18–20] The non-covalent interaction energy part of the large GMTKN30 database[12,21] is mainly based on calculations: Of the 95 noncovalent interaction energies in GMTKN30, only the six noble-gas gas dimer dissociation energies (the RG6 set) are based on experiment.[22,23] Therefore, more high-quality experimental benchmark data for testing dispersion-corrected DFT methods and high-level correlated quantum chemical methods would be highly desirable.[10,24–28]

The intermolecular dissociation energy D_0 of a gas-phase bimolecular complex in its electronic ground state S_0 is such a benchmark observable. However, the number of $D_0(S_0)$ measurements of dispersively bound M·S complexes that are accurate enough to serve as benchmarks is quite limited.[10,29–37] Below we present experimental dissociation energies $D_0(S_0)$ of the aromatic molecule 1-naphthol (1NpOH) complexed to a noble gas atom (Ne, Ar, Kr or Xe) or to N_2. We chose these nonpolar "solvents" S because (1) they give rise to complexes that are dominantly bound by London dispersion interactions, (2) they are taken from the second to fifth row of the periodic table, so their electronic polarizabilities change over an order of magnitude, (3) they cover a wide range of weak interactions from < 2.5 to about 11 kJ/mol, and (4) their structural simplicity makes them attractive for testing high-level theoretical methods that have a steep dependence of computational time on the system size.

The 1NpOH moiety is small enough to be treated by high-level theoretical methods but large enough to offer two different intermolecular binding sites: The naphthalene ring gives rise to dispersively bound Face structures,[31–33,38–41] while the OH group can act as a nonclassical hydrogen-bond donor, giving rise to Edge structures.[35,36,40,42] The 1NpOH·N_2 complex is interesting because its spectrum has been previously interpreted in terms of a Face complex,[43] whereas the closely related phenol·N_2 complex forms an Edge structure.[44] For the complexes investigated here, nearly all the dispersion-corrected DFT calculations predict both Face and Edge structures.

The gas-phase S_0 and S_1 state dissociation energies were measured using the stimulated emission pumping-resonant two-photon ionization (SEP-R2PI) method that was developed in the 1990s[31–33,42] and employed to determine the D_0 values of dispersively bound complexes of the aromatic chromophores carbazole[31–34] and 1NpOH.[35,36,42] We recently determined dissociation energies $D_0(S_0)$ of 1NpOH with cycloalkanes ranging from cyclopropane to cycloheptane, which revealed that the D_0 of these complexes is *not* simply proportional to the molecular polarizability of the cycloalkane, but saturates with increasing size of the cycloalkane and depends on the details of the structure of the intermolecular complex.[40,41,45]

Below, we compare the experimental D_0 values to the binding energies D_e and dissociation energies D_0 calculated with the widely-used dispersion-corrected density functional theory (DFT) methods B3LYP-D3, B97-D3 and ωB97X-D. We also calculate the D_0 values of the carbazole complexes with the noble gases and N_2. The availability of nine experimental dissociation energies that are accurate to $\leq 3.5\%$ allows to compare their dependence on (1) the molecular size of the aromatic, (2) the polarizability of S, and (3) to benchmark the dispersion-corrected DFT calculated values vs. the experimental D_0 energies.

II. METHODS

A. The SEP-R2PI Method

Very briefly, a $\sim$ 5 ns pulsed tunable UV *pump* laser is fixed at a cold band that originates from the $S_0; v'' = 0$ vibrational ground state of the 1NpOH·S complex, exciting it to either the vibrationless $S_1; v' = 0$ level (0_0^0 band) or to a low-frequency intermolecular vibrational level. After a short delay of $1 - 3$ ns, a tunable *dump* laser stimulates resonant vibronic transitions back down to vibrationally excited levels ($v_i'' > 0$) of the S_0 state. The dump laser is scanned to smaller

wavenumber than the 0_0^0 transition; whenever it is resonant with a $S_1; v' = 0 \rightarrow S_0; v_i'' > 0$ downward transition, a large part of the $S_1; v' = 0$ population is transferred to a specific vibrationally excited $v_i'' > 0$ level. The resulting "microcanonically hot" 1NpOH·S complexes undergo intra- and intermolecular vibrational redistribution (IVR) from this v_i'' level into all other energetically accessible vibrational states. After a long delay ($3-5$ μs) that allows IVR to go to completion, the hot 1NpOH·S complexes are detected by R2PI with a third pulsed UV dye laser, denoted the *probe* laser. We have previously shown that this delay is long enough to permit all initially prepared S_0 vibrational levels to couple to the intermolecular dissociation coordinates.[41]

For the D_0 measurement, the probe laser is fixed to a cold transition between the $v'' = 0$ level and either the $v' = 0$ level (0_0^0 band) or to a low-lying intermolecular vibrational level $S_1(v'_{inter} > 0)$. When scanning the dump laser, the resonant dump transitions are detected as a *decrease* of the probe laser signal, because the $v'' = 0$ population is additionally depleted via the pump/dump population transfer to $v_i'' > 0$ levels. Such a *cold-band* SEP-R2PI spectrum looks qualitatively similar to the dispersed fluorescence spectrum from the $S_1(v' = 0)$ level of the 1NpOH·S complex, but with negative-going peaks.

Conversely, if the probe laser is fixed at a hot band (or sequence band) that originates from a $v'' > 0$ level, we obtain a positive-going *hot-band* SEP-R2PI signal. Scanning the dump laser while detecting the hot-band SEP signal gives a hot-band SEP-R2PI spectrum that *increases* at every resonant dump laser transition, since the hot level being probed is populated via IVR. Hot-band SEP signals are only observed as long as the hot 1NpOH·S complex remains bound during the delay time between the dump and probe laser transitions. When the dump laser excites vibrational levels of the 1NpOH moiety that are energetically above than the S_0 dissociation energy of the complex, IVR is followed by efficient 1NpOH $\leftrightarrow$ S vibrational predissociation. The hot 1NpOH·S complex is no longer formed, so the hot-band signal is no longer detected with the probe laser. The ground-state dissociaton energy $D_0(S_0)$ of the complex is then bracketed between the highest-wavenumber dump transition that is observed in the hot-band SEP spectrum and the next higher vibration that appears in the cold-band SEP spectrum (or in the fluorescence spectrum) but does *not* appear in the hot-band SEP spectrum.

B. Experimental

The supersonically cooled 1NpOH·S complexes were produced by co-expanding 1NpOH (Fluka, 99%) and 1% Ar, 0.8% Kr, 0.5% Xe or 1% N_2 which were premixed in Ne carrier gas; the total backing pressure was $1.4 - 1.6$ bar. The 1NpOH·Ne complex was produced by expansion in neat Ne. The 1NpOH was heated to 353 K (0.5 mbar vapor pressure). Two frequency-doubled tunable dye lasers (Lambda Physik FL2002 and FL3002, fundamental range $620 - 660$ nm) were employed as pump ($\sim$ 0.5 mJ/pulse) and dump ($\sim$ 2 mJ/pulse) lasers. Both were pumped by the same Nd:YAG laser (Quanta Ray DCR3). The probe dye laser (Lambda Physik LPD 3000, ~ 0.3 mJ/pulse) was pumped by a Continuum Surelite II frequency-doubled Nd:YAG laser. The dye-laser wavelength and bandwidths before frequency doubling were monitored using a HighFinesse WS6 wavemeter; the bandwidths were $0.3 - 0.4$ cm^{-1}. The probe laser was time-delayed by $3 - 5$ μs and crossed the molecular beam $3 - 5$ mm downstream of the pump and dump lasers, to compensate for the ~ 950 m/s mean speed of the molecular beam. Other experimental details were reported previously .[40,41]

Mass-selective one-color resonant two-photon ionization (R2PI) spectra were recorded using a 120 cm long linear time-of-flight mass spectrometer. Mass-selective ion signals were measured for all complexes. UV/UV hole-burning spectroscopy was performed; for the Ar, Kr and Xe complexes only one ground-state isomer was observed, whereas two ground-state species were observed for the Ne and N_2 complexes.

In the one-color R2PI process, the ionization laser (with the same photon energy as the excitation laser) may deposit sufficient energy in the ground state of the ionized complex to induce dissociation in the ion state. Larger 1NpOH·S_n clusters were present in small relative amounts. The R2PI spectra of the 1NpOH·S_n ($n = 2, 3$) clusters were also measured to evaluate the possibility of fragmentation in the ion state into the respective $(n-1)^+$ ion channels. No evidence was found to suggest that this occurs to a significant degree.

$S_1 \rightarrow S_0$ dispersed fluorescence spectra were measured by exciting the respective 0_0^0 band or intermolecular fundamental excitation (in some cases). The fluorescence was collected with fused silica optics and detected in the second order of a SOPRA UHRS F1500 1.5 m monochromator using a Hamamatsu R928 photomultiplier. The slit width was 200 μm, equivalent to a bandpass of 28 pm; the spectra were scanned in 2.5 pm steps.

C. Computational

The geometrical structures, harmonic vibrational wavenumbers, binding energies (D_e) and dissociation energies (D_0) of the 1NpOH·S and carbazole·S complexes were calculated using the B97 density functional with the D3 dispersion correction[16,17] (B97-D3) and the def2-TZVPP basis set, using Gaussian 16 (Rev. A).[46] B97-D3 exhibits one of the smallest total mean absolute deviations (MAD) between experiment and calculation for the noncovalent interaction part of the GMTKN30 test set.[12] The B97-D3 method also predicts that Ne_2 is a bound molecule, in contrast to the dispersion-corrected GGA functionals BP86-D3, BPBE-D3, and BOP-D3.[12] This property is important, since we experimentally investigate the 1NpOH·Ne complex. Also, the B97-D3 dissociation energies of the previously measured 1NpOH·cycloalkane complexes agreed with the experimental values to within $\leq 1.1\%$.[40,41]

For comparison, additional calculations were performed with the B3LYP-D3 method and the def2-TZVPP basis set, and with the ωB97X-D method[15] (which employs the D2 dispersion correction) and the 6-311++G(d,p) basis set for all complexes except for the Xe complex, for which the def2-TZVPP basis set was used. For Xe, the def2-TZVPP basis set[47] models the inner shell electrons with the small-core effective-core potential ECP-28,[48] which represents the core AOs from 1s to 3d. The counterpoise method for correcting D_e values for basis-set superposition error is not recommended if the D3 method is used,[16] and thus it was not employed with B97-D3 and B3LYP-D3. The ωB97X-D results were counterpoise corrected.

The structure optimizations were unconstrained. The threshold for SCF convergence was set to 10^{-9} a.u., the convergence threshold for RMS Force to 10^{-6} a.u., maximum Force to $2x10^{-6}$ a.u., the RMS displacement to $4x10^{-6}$ a.u. and the maximum displacement to $6x10^{-6}$ a.u. (corrresponding to the VERYTIGHT option in Gaussian16).[46] The optimized minima were checked for the absence of imaginary vibrational frequencies. The Cartesian coordinates of the ground state geometries of 1-naphthol and of all the Face and Edge complexes optimized with all three DFT methods are given in Tables S1-S33 (supplementary material, SI).

The harmonic frequencies and vibrational zero point energies (VZPE) of the monomers and complexes were calculated at the respective optimized structures. Based on these we calculated the change of VZPE, ΔVZPE = VZPE(complex) – VZPE(1NpOH) –VZPE(S). This consists of a contribution from the intermolecular vibrations that arise in the complex (three for the noble gases, five for S=N_2); the other contribution arises from the *change* of the intramolecular vibrational

wavenumbers of 1NpOH and of S (for S=N_2). The dissociation energies are then calculated as $D_0 = D_e - \Delta$VZPE.

III. RESULTS

A. R2PI spectra

Figure 1 shows the one-color R2PI spectra of bare 1-naphthol and the 1-naphthol·S complexes in the region of their $S_0 \rightarrow S_1$ 0_0^0 bands. The spectra of the complexes, Figure 1(b-g), exhibit weak bands corresponding to low-frequency intermolecular vibrational fundamentals and their overtones or combinations. These give valuable information about the intermolecular frequencies and VZPEs and will be discussed in section IV D.

The 0_0^0 bands of the complexes are shifted relative to the 0_0^0 of bare 1-naphthol (at 31455 cm^{-1}) by the spectral shift $\delta\tilde{\nu}$. Assuming that the $S_0 \rightarrow S_1$ electronic excitation is localized on the 1NpOH moiety, the spectral shift corresponds to the difference of ground- and excited-state dissociation energies, $\delta\tilde{\nu} = D_0(S_0) - D_0(S_1)$.[31–33,35,42] The R2PI spectra of 1NpOH·Ar and 1NpOH·N_2 have been measured previously by Zierhut et al,[43] who reported spectral red shifts of $\delta\tilde{\nu} = -15$ cm^{-1} for S=Ar and -14 cm^{-1} for S=N_2.[43] The spectral shift of the of 1NpOH·S complexes also indicates their binding topology: If cyclopropane is dispersively adsorbed as a Face complex, the spectral shift is small or even to the blue ($\delta\tilde{\nu} = +1.9$ cm^{-1}), while in the hydrogen-bonded OH$\cdots$cyclopropane Edge complex, the spectral shift is large and to the red ($\delta\tilde{\nu} = -71.5$ cm^{-1}).[40] The small spectral shifts of the complexes reported here imply that the noble gas or N_2 is adsorbed in a Face geometry.

1-Naphthol·Ne: UV/UV spectral holeburning experiments on the Ne complex revealed a contribution from a minor species whose $S_0 \rightarrow S_1$ 0_0^0 band is slightly blue-shifted relative to that of 1NpOH. Figure 1(b) shows the spectrum of the major 1NpOH·Ne species in the jet, the spectral contribution of the minor species has been removed by UV/UV hole-burning. The spectrum is dominated by the 0_0^0 band, which is shifted by $\delta\tilde{\nu} = -2$ cm^{-1}. The small shift implies a small change between the S_0- and S_1-state dissociation energies and leads us to assign this species as a Face isomer. Weak intermolecular excitations are observed at $0_0^0 + 11$ cm^{-1} and $0_0^0 + 37$ cm^{-1}. Their low Franck-Condon factors imply a small change of geometry between the S_0 and S_1 state

for the Ne complex. The B97-D3 frequency calculations in Table I predict the three intermolecular fundamental vibrations at 8.5 cm^{-1} (in-plane long-axis ν_X), 13.2 cm^{-1} (in-plane short-axis vibration ν_Y) and at 39.8 cm^{-1} (perpendicular ν_Z vibration). Given the small change in geometry and dissociation energy, we expect the calculated S_0 state harmonic wavenumbers to be similar to the calculated S_1 values. Indeed, the observed bands at 11 and 37 cm^{-1} agree well with the calculated ν_X and ν_Z wavenumbers. The experimental and calculated S_0 state harmonic wavenumbers of the intermolecular vibrations are compared in Table I.

Since the spectrum of the minor species overlaps extensively with that of the major species it is hard to separate cleanly; the total 1NpOH·Ne R2PI spectrum and the partially separated UV/UV-holeburned spectra are shown in Figure S1 (supplementary material). The minor species could either be a second ground-state Face isomer or residual population of S_0 state $\nu_X = 1$ level. Assuming a typical vibrational temperature $T_{vib} \sim 10$ K in the supersonic jet expansion, we would expect a relative population of $20 - 30$ % in $v_X = 1$, which agrees nicely with the observed intensity of the minor species.

1-Naphthol·Ar: The R2PI spectrum in Figure 1(c) shows an intense $S_0 \rightarrow S_1$ electronic origin band at 31440 cm^{-1} and five intermolecular vibronic transitions. The UV/UV holeburning measurements reveal that all bands originate from one single isomer. The 0_0^0 band is shifted by $\delta\tilde{\nu} = -14.8$ cm^{-1} relative to 1NpOH, very close to the value reported previously.[43] The bands at 7.3, 19.8 and 46.1 cm^{-1} above the origin are assigned to the three intermolecular fundamental vibrations ν'_X, ν'_Y and ν'_Z, based on the calculated intermolecular B97-D3 frequencies in Table I. The experimental ν'_X wavenumber is only 65 % of the calculated ν_X value. However, the ν'_Y and ν'_Z wavenumbers agree withing $3 - 5$ % with the calculated values, see Table I. The two bands at 14.8 and at 37.2 cm^{-1} are assigned to the $2\nu'_X$ and $2\nu'_Y$ overtone transitions.

1-Naphthol·Kr: The 1NpOH·Kr spectrum is shown in Figure 1(d). The intense $S_0 \rightarrow S_1$ origin at 31433 cm^{-1} is shifted by $\delta\tilde{\nu} = -22$ cm^{-1} relative to 1NpOH. UV/UV holeburning spectroscopy also revealed only a single isomer. Similar to the Ar complex, five intermolecular vibronic bands are observed. The three bands at 8.2, 20.4 and 42.4 cm^{-1} above the origin are assigned to the intermolecular fundamentals ν'_X, ν'_Y and ν'_Z by comparison to the B97-D3 calculated wavenumbers. As Table I shows, the agreement of the experimental and calculated wavenumbers is good, the ν'_X value being in better agreement with calculation than in the Ne and Ar complexes; also, ν'_Z is

1.8 cm^{-1} higher than calculated. The two bands at 16.7 and 36.2 cm^{-1} are assigned to $2\nu'_X$ and $2\nu'_Y$. The latter lies 5 cm^{-1} below the value expected for a harmonic overtone $2\nu'_Y = 40.8$ cm^{-1}. Since this value nearly coincides with the calculated B97-D3 $\nu'_Z = 40.6$ cm^{-1} wavenumber, one expects that these two levels may give rise to a 2:1 Fermi resonance, leading to downward and upward frequency shifts of the $2\nu'_Y$ and ν'_Z levels relative to the uncoupled harmonic values.

1-Naphthol·Xe: Figure 1(e) shows the R2PI spectrum of 1NpOH·Xe. The intense 0^0_0 band at 31420 cm^{-1} is red-shifted by $\delta\tilde{\nu} = -35$ cm^{-1} relative to bare 1NpOH. The bands at 10.5, 22.5 and 37.5 cm^{-1} above the origin are assigned to the intermolecular vibrational fundamentals ν'_X, ν'_Y and ν'_Z, by comparison with the B97-D3 calculated values, given in Table I. The agreement of the calculated harmonic ν_X and ν_Y wavenumber with experiment is very good; the experimental ν'_Z is 5.4 cm^{-1} lower than calculated. Since the experimental ν'_Y is at 22.5 cm^{-1}, the harmonic $2\nu'_Y$ overtone should lie at ~ 45 cm^{-1}, where a weak band is indeed observed. We suggest that the $2\nu'_Y \leftrightarrow \nu'_Z$ Fermi resonance interaction is smaller than in the 1NpOH·Kr complex, since the the Y^2_0 band is much less intense than the Z^1_0 band.

1-Naphthol·N_2: The one-color R2PI spectrum of the 1NpOH·N_2 complex is shown in Figure S2(a) (SI); it differs from those of the noble-gas complexes in that the most intense band at 31441 cm^{-1} is *not* at lowest wavenumber; two additional bands are observed further to the red. A similar 1C-R2PI spectrum of 1NpOH·N_2 complex was measured and discussed by Zierhut et al.,[43] who assigned the most intense band at 31441 cm^{-1} as the 0^0_0, but did not discuss the lower-lying bands. They performed UV/UV holeburning experiments (not shown there) and reported that it was "difficult to extract detailed information".[43] Our UV/UV holeburning experiments revealed separate spectral contributions from two species that we denote isomer 1 and 2; their UV-holeburned spectra are shown in Figure 1(f) and (g). The 1C-R2PI spectrum and the two separated UV/UV holeburning spectra of isomers 1 and 2 are shown in the Figure S2 (supplementary information). Under the expansion conditions used for Figure 1(f,g) the 0^0_0 band intensity of isomer 1 is nearly three times that of isomer 2; this intensity ratio can be varied between about $2:1$ to $5:1$, depending on backing pressure.

We assign the intense band at 31441 cm^{-1} as the 0^0_0 band of isomer 1. It is shifted by $\delta\tilde{\nu} = -14.4$ cm^{-1} to the red of the 1NpOH origin, close to the value reported by Zierhut et al., [43] and also similar to the shift of the Ar complex, see Figure 1(c). The spectral shift of the 0^0_0 band of

isomer 2 is $\delta\tilde{\nu} = -28$ cm^{-1}, which is close to twice that of red shift of isomer 1. This might suggest that the species 2 actually arises from $n = 2 \rightarrow 1$ fragmentation of the $n = 2$ cluster (or cluster ion), the corresponding spectral signal then appearing in the $n = 1$ ion channel. This was investigated by measuring the 1C-R2PI spectra of 1NpOH and the 1NpOH·$(N_2)_n$ clusters with $n = 1-3$ at the same time. No spectroscopic signature of the $n = 1 \rightarrow 0$ fragmentation appears in the mass channel of bare 1NpOH$^+$ and at the same time, the spectrum measured in the $n = 2$ ion mass channel is completely different from that measured in the $n = 1$ mass channel. In order to attribute the spectrum of species 2 to the $n = 2$ cluster we would have to assume that $n = 2 \rightarrow 1$ fragmentation is 100 % efficient while both the $n = 1 \rightarrow 0$ and $n = 3 \rightarrow 2$ fragmentation processes are highly inefficient. This seems very improbable, so we remain with the assignment to a second, structurally distinct Face isomer of the $n = 1$ N_2 complex.

The UV-holeburned spectra of isomers 1 and 2 exhibit similar four- to five-membered vibrational progressions with slightly unequal spacings of about $7 - 9$ cm^{-1}. The lowest harmonic intermolecular frequency of the N_2 complexes calculated with the B97-D3 method is 25 cm^{-1} for the long-axis in-plane vibration ν_X, the other modes are calculated to have even higher frequencies up to 93 cm^{-1}, see Table I. However, the N_2 complex has one intermolecular vibrational degree of freedom that corresponds to internal rotation of the N_2 about an axis perpendicular to its internuclear axis and parallel to the surface normal of the naphthalene ring, similar to the internal rotation modes of the complexes of N_2 with aniline,[49], benzene,[50] and p-difluorobenzene.[51] In the benzene·N_2 complex there is a low (0.05 cm^{-1}) sixfold V_6 barrier to this motion, so the internal rotation about the C_6 axis is essentially free.[50] In the aniline·N_2 and p-difluorobenzene·N_2 complexes, the lower symmetry of the substrate leads to twofold barriers, but these are also low ($V_2 = 25$ cm^{-1} and $V_2 = 10$ cm^{-1}, respectively).

Assuming that internal rotation is nearly free in 1NpOH·N_2, one expects to observe level energies $E = F \cdot l^2$, where $F = 1.989$ cm^{-1} is the reduced internal-rotation constant of the complex and $l = 0, \pm1, \pm2...$ is the quantum number of internal rotation. The levels are predicted to lie at 2 cm^{-1} ($l = \pm1$), 8 cm^{-1} ($l = \pm2$), 18 cm^{-1}($l = \pm3$) and 32 cm^{-1} ($l = \pm4$). Interestingly, this pattern fits quite well to the observed spectrum of 1NpOH·N_2, see Figure 1(f): The transition to the $l = \pm1$ levels could give rise to shoulder on the blue side of the 0_0^0 band. The transition to the $l = \pm2$ levels fits nicely to the observed band at 9 cm^{-1}. The $l = \pm3$ internal-rotation transition appears at 16.3 cm^{-1}, about 1.7 cm^{-1} lower than expected. However, there may be an Fermi resonance between the ν_X vibrational level, which we assign to the transition at 25 cm^{-1},

and the $l = \pm 3$ level; this pushes the two states apart. The weak band at $0_0^0 + 34.5$ cm^{-1} nicely agrees with to the $l = \pm 4$ internal-rotation transitions that are expected at 32 cm^{-1}.

Thus, three low-frequency bands in the R2PI spectrum of 1NpOH·N_2 that cannot be interpreted in terms of the calculated intermolecular normal-mode frequencies are nicely compatible with the hypothesis that internal rotation of the N_2 moiety is only unhindered or slightly hindered in the S_1 states of isomers 1 and 2. A consequence of the internal-rotation character of this mode is that its contribution to the VZPE is close to zero, in contrast to the normal-mode value of $72.6/2 = 36.3$ cm^{-1} at the B97-D3 level. As discussed in section IV D, we expect the anharmonic VZPE of the N_2 complexes to differ by $0.4 - 0.5$ kJ/mol from the calculated harmonic VZPE.

B. Excited-state lifetimes and intersystem crossing

In the SEP-R2PI process, the $S_1(v' = 0) \rightarrow S_0$ dump laser transition competes with three other excited-state processes of the 1NpOH chromophore, the $S_1 \rightarrow S_0$ internal conversion (IC), $S_1 \rightarrow T_n$ intersystem crossing (ISC) to the energetically accessible triplet states, and $S_1 \rightarrow S_0$ spontaneous fluorescence, with rate constants denoted k_{IC}, k_{ISC} and k_{rad}, respectively. Changing the chemical identity of S leads to dramatic changes in the ISC kinetics of the 1-naphthol chromophore, which we briefly discuss in this section.

We measured the fluorescence lifetimes τ_{fl} of 1NpOH and the complexes at their respective 0_0^0 bands, see above. Laser stray light was eliminated by measuring the fluorescence through the monochromator. Table II shows the experimental lifetimes and the fluorescence quantum yields of the complexes, relative to that of bare 1NpOH. The experimental lifetime of 1NpOH at its $S_0 \rightarrow S_1$ 0_0^0 band is $\tau_{fl} = 61 \pm 3$ ns, in very good agreement with the previous values measured by ns pulsed laser excitation,[52], by time-correlated single photon counting[53], and by ps pump-probe measurements.[54]

Upon complexation of 1NpOH with N_2, the fluorescence lifetime remains the same within the experimental error bars. The lifetime of the Ne complex could not be measured because of the spectral overlap of its 0_0^0 band with that of bare 1NpOH, whose emission swamps that of the 1NpOH·Ne complex. For the Ar complex a lifetime shortening by 25 % is observed, for Kr the lifetime decreases by a factor of 10 and for Xe by a factor of 30 or more.

These decreases reflect the external heavy-atom effect (EHAE) in dispersively bound complexes, first observed by Jortner and co-workers in complexes of tetracene and pentacene with no-

ble gas atoms.[55–59] Mackenzie and co-workers have later studied the EHAE in p-difluorobenzene·S and toluene·S complexes and compared the measured lifetimes to calculated $S_1 \leftrightarrow T_1$ spin-orbit coupling (SOC) matrix elements.[60,61] Based on these results, we suggest that the observed lifetime decrease by a factor of about 30 arises from the spatial proximity of the noble gas atoms with large SOC matrix elements (Ar and especially Kr and Xe) that increase the ISC rate of the 1-naphthol chromophore. This in turn strongly affects the efficiency of the SEP-R2PI experiment and leads to considerably lower signal/noise ratios in the S=Kr and Xe spectra, as will be seen below.

C. Experimental Dissociation Energies

1-Naphthol·Ne: Figure 2(a) shows the hot-band probed SEP-R2PI spectrum of the 1NpOH·Ne complex with the probe laser set to $0_0^0 - 26$ cm^{-1}. This spectrum does not exhibit a single band. This implies that even the lowest-energy vibration that appears at 281 cm^{-1} in the dump spectrum, see Figure 2(b), lies above the ground-state dissociation energy $D_0(S_0)$. Hence, the upper limit to the binding energy is $D_0(S_0) < 281$ cm^{-1} ($D_0 < 3.36$ kJ/mol). This is in agreement with the calculated dissociation energies of the Ne complex which lie between 1.71 and 3.31 kJ/mol, see below. On the other hand, this measurement shows that the lowest D_0 that can be determined by the SEP-R2PI method is limited by the lowest energy vibration of the chromophore that is vibronically active in the $S_0 \leftrightarrow S_1$ spectrum.

1-Naphthol·Ar: Figure 3(a) shows the hot-band probed SEP-R2PI spectrum of the 1NpOH·Ar complex, which was measured with the probe laser set to an intense hot-band signal at $0_0^0 - 27$ cm^{-1}. The R2PI spectrum of pump/dumped 1NpOH·Ar in which the $0_0^0 - 27$ cm^{-1} probe laser position is marked is shown in supplementary Figure S3 (supplementary information). The dump spectrum of 1NpOH·Ar in Figure 3(b) is similar to the hot-band SEP spectrum in Figure 3(a) up to 470 cm^{-1}. However, the highest-energy band in the hot-band SEP spectrum is at 470 cm^{-1}, the next band at 478 cm^{-1} and all following vibronic bands to higher energy in the dump spectrum (b) are *not* observed in (a). Thus, the 470 cm^{-1} and the 478 cm^{-1} bands in Figure 3 bracket the ground-state $D_0(S_0)$ of the 1NpOH·Ar complex as 474 ± 4 cm^{-1}. The $\pm$ value is the width of the bracketing interval and *not* the statistical standard deviation of the experimental mean value of the measurement. The true dissociation energy may lie anywhere within the bracketed interval with equal probability. The excited-state dissociation energy $D_0(S_1)$ is obtained by subtracting the experimental spectral shift of the origin band ($\delta\tilde{\nu} = -14$ cm^{-1}, see section III. A) from the

$D_0(S_0)$ value, giving $D_0(S_1) = 488 \pm 5$ cm^{-1}, see also Table III.

1-Naphthol·Kr: Figure 4(a) shows the hot-band probed SEP-R2PI spectra of the 1NpOH·Kr complex, with the pump laser set to the the intermolecular excitation at $0_0^0 + 36$ cm^{-1} [see Figure 1(d)] and the probe laser set to $0_0^0 - 34$ cm^{-1}, where an intense hot-band signal is observed after dumping. The corresponding R2PI spectrum is shown in Figure S4 (supplementary information). Figure 4(b) shows the analogous hot-band probed SEP-R2PI with the pump laser set to the 0_0^0 band (the probe laser is again set to $0_0^0 - 34$ cm^{-1}). In both traces a clear breaking-off of the spectra is observed. When exciting at the 0_0^0 band we observe the highest-energy transition at 582 cm^{-1}, while if the σ_0^1 band is excited, the highest-energy band is observed at 608 cm^{-1}, see Figure 4(a). Figure 4(c) shows the dump spectrum measured at the 0_0^0 band. The lowest-energy vibronic band that is *not* observed in Figure 4(a) lies at 620.3 cm^{-1}. Thus, the bands at 608 cm^{-1} in Figure 4(a) and 620 cm^{-1} in Figure 4(c) bracket the $D_0(S_0)$ of the 1NpOH·Kr complex as 614 ± 6 cm^{-1}, see Table III. From the spectral shift $\delta\tilde{\nu}$ of 1NpOH·Kr we obtain the excited-state dissociation energy $D_0(S_1) = 636 \pm 65$ cm^{-1}, see also Table III.

1-Naphthol·Xe: As discussed in section III. B, the Xe complex has a very short fluorescence decay lifetime of $\tau_{fl} \leq 3$ ns, due to the heavy-atom induced ISC, which becomes the most effective nonradiative pathway, see Table II. For this reason, the stimulated-emission step is much less efficient and both the dump spectrum and the origin-probed SEP-R2PI spectrum exhibited a much lower S/N ratio compared to the other complexes. Despite the the low fluorescence quantum yield, the best information on the S_0 state vibrations could be obtained from the fluorescence spectrum, which is shown in Figure 5(b).

The hot-band detected SEP spectrum was measured 19 cm^{-1} below the 0_0^0 band, where a weak signal increase occures upon dumping to the S_0 state. A corresponding R2PI spectrum is shown in Figure S5 (supplementary information). The highest-wavenumber transition in this spectrum is observed at 880 cm^{-1}, see Figure 5(a). It clearly correlates with the intense band at 880 cm^{-1} in the fluorescence spectrum. The next higher band in the fluorescence spectrum at 927 cm^{-1} is not observed in the hot-band SEP spectrum, nor are any of the higher energy fluorescence bands. This brackets the $D_0(S_0)$ of the 1NpOH·Xe complex between these two bands as 904 ± 24 cm^{-1}, see Table III. The excited-state dissociation energy is $D_0(S_1) = 939 \pm 24$ cm^{-1}, see also Table III.

1-Naphthol·N_2: As discussed above, two isomers of the 1NpOH·N_2 complex were observed by UV/UV holeburning. The top panel of Figure 6 shows two hot-band probed SEP-R2PI spectra of isomer 1. The red spectrum (a) was excited at an intermolecular vibrational combination band at

$0_0^0 + 34.5$ cm^{-1}, as indicated with a vertical arrow in Figure 1(f). The black spectrum in Figure 6(b) is the hot-band probed SEP-R2PI spectrum following excitation at the 0_0^0 band. In both cases the probe laser was set to $0_0^0 - 53$ cm^{-1}. While the black spectrum exhibits better signal/noise, the highest vibronic excitation that is clearly above the noise is at 545 cm^{-1}, while spectrum (a) shows the highest-energy band at 558 cm^{-1}, thereby significantly increasing the lower limit of $D_0(S_0)$. For the upper D_0 limit we compare to the fluorescence spectrum in Figure 6(c), the lowest-wavenumber band that is not observed in spectrum (b) lies at 571 cm^{-1}. These two values bracket the $D_0(S_0)$ of isomer 1 of the N_2 complex as 565 ± 7 cm^{-1}, given also in Table III.

The corresponding spectra for isomer 2 of the 1NpOH·N_2 complex are shown in the lower panel of Figure 6. We could only measure the hot-band SEP spectrum excited at the 0_0^0 band, Figure 6(d), which is compared to the fluorescence spectrum of isomer 2, shown in Figure 6(e). This spectrum is less well resolved than that of isomer 1, because of the lower concentration of isomer 2 in the supersonic jet. The D_0 of isomer 2 is bracketed between the highest-energy band in the hot-band probed SEP-R2PI (at 535 cm^{-1}) and the next higher-energy band in the fluorescence spectrum, see Figure 6(e) at 571 cm^{-1}, giving $D_0(S_0) = 553 \pm 18$ cm^{-1}.

As Table III shows, the dissociation energies of the two N_2 isomers overlap within their respective brackets. If we assume typical supersonic-jet vibrational temperatures in the range $T_{vib} = 10 - 15$ K, the $\sim 30\%$ intensity of isomer 2 relative to isomer 1 (see Figure 1) implies that the D_0 of isomer 2 is about $8-12$ cm^{-1} smaller than that of isomer 1. This estimate is compatible with the difference of ~ 12 cm^{-1} between the two interpolated D_0 values. Due to the larger spectral shift $\delta\nu$ of isomer 2 relative to that of isomer 1, the S_1 state dissociation energies of the two isomers become very similar, being $D_0(S_1) = 579$ cm^{-1} for isomer 1 and 581 cm^{-1} for isomer 2, see also Table III.

D. Calculated Structures

The B97-D3, B3LYP-D3 and ωB97X-D calculated structures of the 1NpOH·S complexes are very similar to each other. Since the dissociation energies calculated with B97-D3 are on average closer to the experimental ones than those calculated by the other methods, we only show the B97-D3 structures here. The calculated Cartesian coordinates of all the complexes using all three methods are given in Tables S1-S33 (SI).

Figure 7 shows the calculated Face structures. The noble-gas atoms and the N_2 molecule are

adsorbed above the naphthalene ring at $R_\perp = 3.44$ Å for Ne, 3.56 Å for Ar, 3.62 Å for Kr, 3.75 Å for Xe, 3.13 Å for N_2 isomer (1) and 3.13 Å for isomer 2. Regarding the X/Y coordinates of the structures, the Ne atom is adsorbed directly above the central C8-C9 bond of the naphthalene moiety and is very slightly shifted towards the OH group. With increasing van-der-Waals radius the larger noble gas atoms shift progressively away from the central C8-C9 bond and towards the center of the OH-carrying benzene ring.

With the exception of the Xe complex calculated with the B3LYP-D3 method and the Ar and Xe complexes calculated with the ωB97X-D method, all three DFT methods also predict Edge isomers,[40] in which the -OH group of 1NpOH forms a non-conventional OH$\cdots$S hydrogen bond to the noble-gas atom or N_2 molecule, which now lies in the 1NpOH plane. These Edge structures are shown in the supplementary Figure S6 (supplementary material). However, the calculated ground-state dissociation energies $D_0(S_0)$ are $8 - 40$ % smaller than those calculated for the Face isomers.

IV. DISCUSSION

A. Complex structures and spectral shifts

Zierhut et al. previously observed small spectral shifts of of the $S_0 \rightarrow S_1$ origin bands $\delta\tilde{\nu} = -15$ cm^{-1} and -14 cm^{-1} for the 1NpOH·Ar and 1NpOH·N_2 complexes, respectively, and considered the Ar or N_2 moiety to be adsorbed on the aromatic face of 1NpOH.[43] We have previously noted that the Face isomer of 1NpOH·cyclopropane exhibits a small spectral shift to the blue, $\delta\tilde{\nu} = +2$ cm^{-1},[40] while the spectral shift of the Edge isomer of 1NpOH·cyclopropane shows a much larger spectral red shift of -71.5 cm^{-1}.[40] Since the spectral shifts of the noble gas complexes lie between -2 and -35 cm^{-1}, we assign them to Face complexes.

We expect that the Edge isomers predicted by the DFT calculation would show larger red shifts than the Face isomers. However, we have not observed any strongly red-shifted bands, see Figure 1. We therefore conclude that even if such locally stable Edge isomers are formed during the supersonic-jet expansion, they easily isomerize to the more stable Face counterparts.

B. Experimental dissociation energies

We complement the experimental D_0 values of the 1NpOH·S complexes with those of the carbazole·S complexes. These have been measured earlier to within ± 0.05 kJ/mol, using the same SEP-R2PI technique.[31–34] This doubles the size of the benchmark set and allows interesting comparisons. The experimental D_0 values of the carbazole complexes are given in Table V and are graphically compared to the 1NpOH·S dissociation energies in Figure 8.

For the carbazole·Ne complex only an upper limit to D_0 could be measured, but since the lowest optically active vibration in carbazole is lower than in 1-naphthol, this value of < 2.56 kJ/mol is about 1 kJ/mol lower than for the 1NpOH complex. Figure 8 shows that D_0s of the carbazole complexes with S=Ar, Kr and N_2 are uniformly 12% larger than those of the corresponding 1-naphthol complexes. This agrees with expectations, since carbazole ($C_{12}H_9N$) has two second-row atoms more than 1-naphthol ($C_{10}H_8O$), thereby increasing the number of valence electrons and electronic polarizability.

Figure 8 also shows that the experimental D_0 of the carbazole·Xe complex[33] lies at the low limit of the D_0 range measured for 1NpOH·Xe. This seems inconsistent with the relative D_0 values of the carbazole and 1NpOH complexes with Ar, Kr and N_2, and suggests that this D_0 value should be critically reexamined.

C. Comparison of calculated and experimental dissociation energies

Table IV gives the dissociation energies of the 1-naphthol·S complexes that were calculated using the three dispersion-corrected DFT methods; those of the corresponding carbazole complexes are given in Table V. We compare the experimental D_0 values to the calculated ones in Figure 9.

Starting with the 1-naphthol·Ne complex, one sees that the experimental upper D_0 limit is larger than all the calculated values, so the experiment is compatible with all calculations, but does not test them. The D_0 of 1NpOH·Ar is closest to the B97-D3 value, the B3LYP-D3 calculated D_0 being 13% too high, while the ωB97X-D D_0 is 9% too low. For the N_2 complex we compare the calculated and experimental values for isomer 1 because of the narrower experimental brackets for this complex. The experimental D_0 is closest to the ωB97X-D value, with B97-D3 being 5% larger and B3LYP-D3 about 9% larger. As for Ar, the D_0 of 1NpOH·Kr is also closest to the B97-D3 value, however, the ωB97X-D value is now the second closest, being only 4% too high,

while the B3LYP-D3 D_0 is 15% too high. 1NpOH·Xe is the only complex for which all the DFT calculated D_0 values fall below the experimental value, with B97-D3 predicting the lowest D_0 (-12%), ωB97X-D being closer (-8%) and B3LYP-D3 closest (-4%). Overall, the B97-D3 D_0 values exhibit the smallest mean average deviation (MAD) relative to experiment, followed by the D_0 values calculated by the ωB97X-D and by B3LYP-D3 methods.

Turning to the carbazole·Ne complex in Figure 9(b), again only an upper limit of $D_0 < 2.56$ kJ/mol is known.[33] Interestingly, both the the B3LYP-D3 and B97-D3 calculated D_0 values are larger (by 35 % and 6%, respectively), and only the ωB97X-D value is compatible with experiment. For the Ar, Kr and Xe complexes the B97-D3 calculated D_0 values are closest to the experimental $D_0(S_0)$ values; the MAD is $+0.3$ kJ/mol and the maximum deviation is $+0.65$ kJ/mol. The B3LYP-D3 values are too large by between 12 and 20%. The ωB97X-D method gave erratic results for the carbazole complexes, showing good agreement for S=Ne and N_2 and reasonable agreement for Ar, but failing to converge for Kr and overshooting nearly by a factor of two for the Xe complex.

D. Intermolecular vibrations and vibrational zero-point energies

The calculated dissociation energies are obtained from the calculated binding energies D_e and changes of vibrational zero-point energy, i.e., $D_0 = D_e - \Delta$VZPE. Hence we need to consider the relative size of these two contributions and their respective errors. As discussed in section II C and shown in the last two columns of Table 1, there are two contributions to ΔVZPE: the VZPE of the three intermolecular modes (five for N_2) contributes $70 - 95\%$ of ΔVZPE. The other $5 - 30\%$ ($0.05 - 0.25$ kJ/mol) arise from the changes of the *intra*molecular vibrational frequencies of the 1-naphthol (and N_2) moieties upon complex formation.

Table IV shows that the ΔVZPE is $11 - 14\%$ of D_e for Ne, decreasing to $\sim 9\%$ of D_e for Ar, to $\sim 7\%$ for Kr and to 6.5% of D_e for Xe. For the carbazole·rare-gas complexes, Table V shows that the ratios of ΔVZPE to D_e are very similar. These comparisons show that (1) the VZPE contributions to D_0 are small for the noble-gas complexes, especially for those with heavy atoms; (2) the harmonic treatment of the intermolecular vibrations leads to errors in ΔVZPE that are < 0.1 kJ/mol relative to the experimental values; (3) the ΔVZPE from the changes of the *intra*molecular vibrational frequencies are < 0.1 kJ/mol for the Ne and Ar complexes but increase to 0.25 kJ/mol for the Xe and N_2 complexes.

These findings are in marked contrast to dimers or clusters of small hydride molecules, such as $(H_2O)_2$, $(NH_3)_2$, $(HF)_2$ or $(HCl)_2$ for which the ΔVZPE amounts to $25-40$ % of the D_e and where the theoretical determination of D_0 crucially depends on the anharmonic treatment of VZPE and of ΔVZPE.[62]

In contrast, the N_2 complexes exhibit two additional intermolecular vibrations (the in-plane and out-of-plane internal rotation of N_2). The contributions of ΔVZPE to D_e are $18-21\%$ for the 1-naphthol complex and $17-18\%$ for the carbazole complex, depending slightly on the DFT method, see Tables IV and V. As discussed in section III A, the harmonic treatment of the VZPE of the internal-rotation mode (Table I) is probably in serious error. The calculation predicts $\tilde{\nu}_{ip.rot} = 73$ and 70 cm^{-1} for isomer 1 and 2 , while the observed internal-rotation levels imply that the VZPE for this mode is < 2 cm^{-1}, leading to an overestimate of ΔVZPE by ~ 0.4 kJ/mol. Clearly, the ΔVZPE corrections are substantial (especially for the N_2 complexes) and mandatory for accurate calculations of D_0.

V. CONCLUSIONS

We have determined accurate S_0 and S_1 state intermolecular dissociation energies D_0 for the intermolecular 1-naphthol·S complexes with S= Ne, Ar, Kr, Xe and N_2 (two isomers). Using the stimulated-emission pumping resonant two-photon ionization (SEP-R2PI) method, the S_0 state dissociation energies were bracketed to < 0.3 kJ/mol. The Ar, Kr and N_2 (isomer 1) D_0 values could be determined to within 0.08 kJ/mol, corresponding to a relative uncertainty of ± 1 %. The corresponding S_1 state dissociation energies are obtained by subtracting the $S_0 \rightarrow S_1$ spectral shift of the 0_0^0 bands of the 1-naphthol·S complexes from the respective $D_0(S_0)$ values. Electronic $S_0 \rightarrow S_1$ excitation of the 1-naphthol moiety led only to a small increase of D_0, between $\sim 1\%$ for Ne and $\sim 4-5\%$ for Xe and N_2.

The experimental D_0 values of the 1-naphthol·S complexes S= Ne, Ar, Kr, Xe and N_2 scale approximately linearly with increasing electronic polarizability α of the adatom or admolecule. This result is in agreement with the London model for dispersive interactions between closed-shell atoms.[1,2] For N_2 the linear correlation of $D_0(S_0)$ with α is only good if we plot against the long-axis (parallel) polarizability α_{zz} of N_2, the correlation of D_0 with the perpendicular polarizability α_{xx} is unsatisfactory. Note that for cycloalkane admolecules, which have larger polarizabilities, the D_0 values do not scale *linearly* with the α of S but increase much more slowly and depend on

details of the structure of the admolecule.[41]

The structures, binding energies D_e, vibrational frequencies and changes of vibrational zero-point energy (ΔVZPE) were calculated using the dispersion-corrected density functional methods B97-D3, B3LYP-D3 and ωB97X-D. All methods predict that Face structures are most stable, in which the adatom/molecule is adsorbed above and close to the center of the naphthalene frame, similar to the 1-naphthol·cyclopropane Face isomer.[40] All three DFT-D methods also predict Edge isomers in which the S moiety forms a nonconventional H-bond to the OH group of 1-naphthol, similar to the 1-naphthol·cyclopropane Edge isomer.[40] While B97-D3 predicts stable Face and Edge minima for all complexes, the B3LYP-D3 and ωB97X-D methods predict index-1 saddle points for some adatoms. The calculated dissociation energies of the Edge isomers are smaller than those of the Face isomers, although for the Ne complex the difference is small ($0.1 - 0.25$ kJ/mol). For the larger adatoms/-molecule, the differences increase to $1 - 2.5$ kJ/mol.

Based on the small spectral shifts, we assign the observed R2PI and UV holeburning spectra to Face complexes. We searched for signals of Edge isomers, but did not observe any red-shifted bands with significant intensity. This implies that the Edge$\rightarrow$ Face isomerization barriers are low for these complexes. Using UV/UV holeburning, we were able to separate two spectra for the 1NpOH·N_2. The DFT-D calculations indeed predict two separate Face isomers with the N_2 is adsorbed above either of the benzene rings of 1-naphthol. For the Ne complex, UV holeburning allowed to partially separate the spectrum of a minor species that is blue-shifted by a few cm^{-1} from the 0_0^0 band of the major species. Since all the DFT-D calculations predict a only single S_0 state isomer for the Ne complex, we interpret the minor species in terms of residual population of the S_0 state $v_x = 1$ level.

We extended the calculations to the analogous Ne, Ar, Kr, Xe and N_2 complexes of the planar aromatic carbazole which were previously measured using the SEP-R2PI method.[31–34,63] Again all three DFT-D methods predict Face and Edge complexes. The Face complexes are predicted to be more stable, in agreement with the relatively small experimental spectral shifts. The comparison of the experimental D_0 values of 1-naphthol·Xe and carbazole·Xe revealed that both values lie within the (larger) bracketing limits of the 1-naphthol·Xe D_0, whereas the D_0 trend of the Ne-Kr complexes suggests that the D_0 of carbazole·Xe[33] should be $\sim$ 1 kJ/mol larger than that of 1-naphthol·Xe. This difference needs to be checked in the future.

Based on the nine experimental dissociation energies for the complexes of two different aromatic molecules, we evaluated and compared the predictions of the three DFT methods: Overall,

the B97-D3 method reproduced the experimental D_0 values best, with a mean absolute difference (MAD) of 0.37 kJ/mol and a maximum difference of 1.27 kJ/mol (for 1-naphthol·Xe). This predictive performance is encouraging, but the MAD is significantly larger than the experimental bracketing width, which is ± 0.10 kJ/mol, when averaged over the same nine complexes. The B3LYP-D3 method exhibited a larger MAD of 1.10 kJ/mol and a larger maximum difference of 2.12 kJ/mol (for carbazole·Xe). The ωB97X-D method exhibits the poorest overall agreement with experiment, with a MAD of 2.20 kJ/mol and a largest maximum difference of 11.8 kJ/mol (again for the carbazole·Xe complex). For two of the complexes convergence problems arose with the ωB97X-D calculations, these values are not included in the comparison. Without the -D or -D3 dispersion corrections, none of these complexes are predicted to be bound.

The VZPE contribution to D_0 and the ΔVZPE correction were examined experimentally and theoretically. The calculated intermolecular VZPE is small compared to the intermolecular well depth D_e, being $\sim 11\%$ of D_e for S=Ne and decreasing to $\sim 4\%$ of D_e for the Xe complex. For the 1-naphthol·S complexes with S=Ar, Kr and Xe, for which all three intermolecular vibrations were experimentally observed, the calculated (harmonic) B97-D3 intermolecular VZPE is $4 - 5$ cm^{-1} ($0.05 - 0.06$ kJ/mol) larger than the experimental VZPE. These differences are about 10 times smaller than the differences of calculated and experimental D_0 values discussed above. Thus, for the noble-gas complexes, the differences between calculated and experimental D_0 values are dominated by the errors of the calculated well depths D_e, followed by the experimental bracketing widths, the vibrational ZPE differences between calculation and experiment are the smallest error source. For the N_2 complex five intermolecular vibrations contribute to the intermolecular VZPE. The calculated ΔVZPE is $18 - 25$ % of the D_e, depending on the DFT method. The in-plane internal-rotation mode of the N_2 complexes is very poorly described by the normal-mode treatment: The predicted harmonic frequency is ~ 70 cm^{-1}, while experimentally this vibration is a (slightly) hindered internal rotation, whose lowest excitation lies at $2 - 3$ cm^{-1}. For this mode the calculated and experimental VZPE differ by about 0.4 kJ/mol. The out-of-plane internal-rotation mode of the N_2 moiety was not detected experimentally, so no overall evaluation of the VZPE could be made. We suspect that the relatively good agreement of experimental and calculated D_0s for the N_2 complexes is be due to fortuitous cancellation of errors in the calculated D_e and the calculated ΔVZPE values.

We believe that the nine experimental D_0 values presented above – especially in combination with the experimental D_0 values of the 1NpOH·cycloalkane complexes[40,41] and those of other

intermolecular complexes discussed in the literature[10,37] – can serve as experimental benchmarks for testing both highly correlated *ab initio* calculations and density functional methods, as well as for improving our understanding and modelling of intermolecular interactions.

Supplementary Material

See supplementary material for additional UV/UV-hole-burning and probe laser spectra (Figures S1 to S5), structures of the Edge complexes (Figure S6) and tables of Cartesian coordinates of the 1-naphthol and carbazole complexes optimized by the DFT methods (Tables S1 to S33).

Acknowledgements

We thank the Swiss National Science Foundation for financial support (grant 200021E-160404). Ms. Anja Poblotzki (Universität Göttingen) contributed to the initial measurements on 1NpOH·Ar during a scientific visit to University of Bern that was funded by the Priority Program SPP1807 "*Control of London dispersion interactions in molecular chemistry*" of the DFG.

---

* Department of Atomic and Molecular Physics, Manipal University, Manipal-576104, Karnataka, India

† samuel.leutwyler@dcb.unibe.ch

1 F. LONDON, *Z. Phys.* **63**, 245 (1930).

2 R. EISENSCHITZ and F. LONDON, *Z. Physik* **60**, 491 (1930).

3 G. C. MAITLAND, M. RIGBY, E. B. SMITH, and W. A. WAKEHAM, *Intermolecular Forces: Their Origin and Determination*, Clarendon Press, Oxford, 1981.

4 G. R. DESIRAJU and T. STEINER, *The Weak Hydrogen Bond in Structural Chemistry and Biology*, Oxford University Press, 2001.

5 T. STEINER, *Angew. Chem. Int. Ed.* **41**, 48 (2002).

6 P. E. S. WORMER and A. VAN DER AVOIRD, *Chem. Rev.* **100**, 4109 (2000).

7 M. MONS, I. DIMICOLI, and F. PIUZZI, *Int. Rev. Phys. Chem.* **21**, 101 (2002).

8 P. HOBZA, *Acc. Chem. Res.* **45**, 663 (2012).

9 C. D. SHERRILL, *Acc. Chem. Res.* **46**, 1020 (2013).

10 J. A. FREY, C. HOLZER, W. KLOPPER, and S. LEUTWYLER, *Chem. Rev.* **116**, 5614 (2016).

[11] J. P. WAGNER and P. SCHREINER, *Angew. Chem. Int. Ed.* **54**, 12274 (2015).

[12] L. GOERIGK and S. GRIMME, *Phys. Chem. Chem. Phys.* **13**, 6670 (2011).

[13] L. GOERIGK and S. GRIMME, *J. Chem. Phys.* **132**, 184103 (2010).

[14] S. GRIMME, *J. Comput. Chem.* **27**, 1787 (2006).

[15] J.-D. CHAI and M. HEAD-GORDON, *Phys. Chem. Chem. Phys.* **10**, 6615 (2008).

[16] S. GRIMME, J. ANTONY, S. EHRLICH, and H. KRIEG, *J. Chem. Phys.* **132**, 154104 (2010).

[17] S. GRIMME, *WIREs Comput. Mol. Sci.* **1**, 211 (2011).

[18] P. JUREČKA, J. ŠPONER, J. ČERNY, and P. HOBZA, *Phys. Chem. Chem. Phys.* **8**, 1985 (2006).

[19] T. TAKATANI, E. G. HOHENSTEIN, M. MALAGOLI, M. S. MARSHALL, and C. D. SHERRILL, *J. Chem. Phys.* **132**, 14404 (2010).

[20] R. PODESZWA, K. PATKOWSKI, and K. SZALEWICZ, *Phys. Chem. Chem. Phys.* **12**, 5974 (2010).

[21] W. HUJO and S. GRIMME, *Phys.Chem.Chem.Phys.* **13**, 13942 (2011).

[22] J. F. OGILVIE and F. Y. H. WANG, *J. Mol. Struct.* **273**, 277 (1992).

[23] J. F. OGILVIE and F. Y. H. WANG, *J. Mol. Struct.* **291**, 313 (1993).

[24] K. E. RILEY, M. PITOŇÁK, P. JUREČKA, and P. HOBZA, *Chem. Rev.* **110**, 5023 (2010).

[25] S. GRIMME, A. HANSEN, J. G. BRANDENBURG, and C. BANNWARTH, *Chem. Rev.* **116**, 5105 (2016).

[26] C. HOLZER and W. KLOPPER, *Mol. Phys.* **115**, 2775 (2017).

[27] C. HOLZER and W. KLOPPER, *J. Chem. Phys.* **147**, 181101 (2017).

[28] R. A. MATA and M. A. SUHM, *Angew. Chemie Int. Ed.* **56**, 11011 (2017).

[29] H. J. NEUSSER and H. KRAUSE, *Chem. Rev.* **94**, 1829 (1994).

[30] J. E. BRAUN, T. MEHNERT, and H. J. NEUSSER, *Int. J. Mass. Spec.* **203**, 1 (2000).

[31] T. BÜRGI, T. DROZ, and S. LEUTWYLER, *Chem. Phys. Lett.* **225**, 351 (1994).

[32] T. BÜRGI, T. DROZ, and S. LEUTWYLER, *J. Chem. Phys.* **103**, 7228 (1995).

[33] T. DROZ, T. BÜRGI, and S. LEUTWYLER, *J. Chem. Phys.* **103**, 4035 (1995).

[34] T. DROZ, T. BÜRGI, and S. LEUTWYLER, *Ber. Bunsenges. Phys. Chem.* **99**, 429 (1995).

[35] C. WICKLEDER, T. DROZ, T. BÜRGI, and S. LEUTWYLER, *Chem. Phys. Lett.* **264**, 257 (1997).

[36] C. WICKLEDER, D. HENSELER, and S. LEUTWYLER, *J. Chem. Phys.* **116**, 1850 (2002).

[37] S. HALDAR, R. GNANASEKARAN, and P. HOBZA, *Phys. Chem. Chem. Phys.* **17**, 26645 (2015).

[38] S. LEUTWYLER and J. JORTNER, *J. Phys. Chem.* **91**, 5558 (1987).

[39] N. BEN-HORIN, U. EVEN, J. JORTNER, and S. LEUTWYLER, *J. Chem. Phys.* **97**, 5296 (1992).

[40] S. MAITY, R. KNOCHENMUSS, C. HOLZER, G. FÉRAUD, J. A. FREY, W. KLOPPER, and S. LEUTWYLER, *J. Chem. Phys.* **145**, 164304 (2016).

[41] S. MAITY, P. OTTIGER, F. A. . BALMER, R. KNOCHENMUSS, and S. LEUTWYLER, *J. Chem. Phys.* **145**, 244314 (2016).

[42] T. BÜRGI, T. DROZ, and S. LEUTWYLER, *Chem. Phys. Lett.* **246**, 291 (1995).

[43] M. ZIERHUT, W. ROTH, S. DÜMMLER, and I. FISCHER, *Chem. Phys.* **305**, 123 (2004).

[44] M. S. FORD, S. R. HAINES, I. PUGLIESI, C. E. H. DESSENT, and K. MÜLLER-DETHLEFS, *J. Electron Spectrosc. Rel. Phenomena* **112**, 231 (2000).

[45] R. KNOCHENMUSS, S. MAITY, and S. LEUTWYLER, *Chimia* **71**, 7 (2017).

[46] M. J. FRISCH, G. W. TRUCKS, H. B. SCHLEGEL, G. E. SCUSERIA, M. A. ROBB, J. R. CHEESEMAN, G. SCALMANI, V. BARONE, G. A. PETERSSON, H. NAKATSUJI, X. LI, M. CARICATO, A. V. MARENICH, J. BLOINO, B. G. JANESKO, R. GOMPERTS, B. MENNUCCI, H. P. HRATCHIAN, J. V. ORTIZ, A. F. IZMAYLOV, J. L. SONNENBERG, D. WILLIAMS-YOUNG, F. DING, F. LIPPARINI, F. EGIDI, J. GOINGS, B. PENG, A. PETRONE, T. HENDERSON, D. RANASINGHE, V. G. ZAKRZEWSKI, J. GAO, N. REGA, G. ZHENG, W. LIANG, M. HADA, M. EHARA, K. TOYOTA, R. FUKUDA, J. HASEGAWA, M. ISHIDA, T. NAKAJIMA, Y. HONDA, O. KITAO, H. NAKAI, T. VREVEN, K. THROSSELL, J. A. MONTGOMERY, JR., J. E. PERALTA, F. OGLIARO, M. J. BEARPARK, J. J. HEYD, E. N. BROTHERS, K. N. KUDIN, V. N. STAROVEROV, T. A. KEITH, R. KOBAYASHI, J. NORMAND, K. RAGHAVACHARI, A. P. RENDELL, J. C. BURANT, S. S. IYENGAR, J. TOMASI, M. COSSI, J. M. MILLAM, M. KLENE, C. ADAMO, R. CAMMI, J. W. OCHTERSKI, R. L. MARTIN, K. MOROKUMA, O. FARKAS, J. B. FORESMAN, and D. J. FOX, Gaussian Revision A.03, 2016, Gaussian Inc. Wallingford CT.

[47] F. WEIGEND and R. AHLRICHS, *Phys. Chem. Chem. Phys.* **7**, 3297 (2005).

[48] K. A. PETERSON, D. FIGGEN, E. GOLL, H. STOLL, and M. DOLG, *J. Chem. Phys.* **119**, 11113123 (2003).

[49] M. SCHÄFER and D. W. PRATT, *J. Chem. Phys* **115**, 11147 (2001).

[50] S. LEE, J. ROMASCAN, P. M. FELKER, T. B. PEDERSEN, B. FERNÁNDEZ, and H. KOCH, *J. Chem. Phys.* **118**, 1230 (2003).

[51] M. SCHÄFER, C. KANG, and D. W. PRATT, *J. Phys. Chem. A* **107**, 10753 (2003).

[52] R. KNOCHENMUSS and S. LEUTWYLER, *J. Chem. Phys.* **91**, 1268 (1989).

[53] C. LAKSHMINARAYAN and J. L. KNEE, *J. Phys. Chem.* **94**, 2637 (1990).

[54] J. L. KNEE, L. R. KHUNDKAR, and A. H. ZEWAIL, *J. Chem. Phys.* **87**, 115 (1987).

[55] A. AMIRAV, U. EVEN, and J. JORTNER, *Chem. Phys. Lett.* **67**, 9 (1979).

[56] A. AMIRAV, U. EVEN, and J. JORTNER, *J. Chem. Phys.* **75**, 2489 (1981).

[57] A. AMIRAV, U. EVEN, and J. JORTNER, *J. Phys. Chem.* **85**, 309 (1981).

[58] O. K. ABOU-ZIED, D. R. M. DEMMER, S. C. WALLACE, and R. P. STEER, *Chem. Phys. Lett.* **266** (1997).

[59] L. C. T. SHOUTE, S. HIRAYAMA, and R. P. STEER, *Chem. Phys. Lett.* **338**, 123 (2001).

[60] R. J. DOYLE, R. DA CAMPO, P. R. TAYLOR, and S. R. MACKENZIE, *J. Chem. Phys.* **121**, 835 (2004).

[61] T. A. A. OLIVER, P. R.TAYLOR, R. J. DOYLE, and S. R. MACKENZIE, *J. Chem. Phys.* **127**, 024301 (2007).

[62] A. K. SAMANTA, Y. WANG, J. S. MANCINI, J. M. BOWMAN, and H. REISLER, *Chem. Rev.* **116**, 4913 (2016).

[63] J. BÖSIGER and S. LEUTWYLER, *Chem. Phys. Lett.* **126**, 238 (1986).

[64] J. J. BREEN, L. W. PENG, D. M. WILLBERG, A. HEIKAL, P. CONG, and A. H. ZEWAIL, *J. Chem. Phys.* **92**, 805 (1990).

TABLE I. Experimental and B97-D3 calculated intermolecular fundamental frequencies and vibrational zero-point energies VZPE (in cm^{-1}) of the 1-naphthol·S Face complexes with S=Ne, Ar, Kr, Xe and N_2 (isomers 1 and 2).

										VZPE		
	Experimental freqs.				B97-D3 harmonic freqs.					Experim.	B97-D3 calc.	
Complex	$\tilde{\nu}_X$	$\tilde{\nu}_Y$	$\tilde{\nu}_Z$	$\tilde{\nu}_{ip.rot}$	$\tilde{\nu}_X$	$\tilde{\nu}_Y$	$\tilde{\nu}_Z$	$\tilde{\nu}_{ip.rot}$	$\tilde{\nu}_{oop.rot}$	intermol.	intermol.	Total
Ne	11	-	37		8.5	13.2	39.8			-	30.8	28.4
Ar	7.3	19.8	46.1		11.4	20.3	48.5			36.6	40.1	46.8
Kr	8.2	20.4	42.4		8.9	20.4	40.6			35.5	35.0	47.6
Xe	10.5	22.5	37.5		11.1	23.9	42.9			35.3	39.0	58.5
N_2 (isomer 1)	25	34.5	57	$\sim$2	25.0	32.4	41.4	72.6	92.6	-	132.0	153.8
N_2 (isomer 2)	21.4	-	-	$\sim$2	20.1	32.7	34.6	69.6	87.3	-	122.2	142.1

TABLE II. Experimental fluorescence lifetimes, relative fluorescence quantum yields Φ_{fl} of *trans* 1-naphthol and the 1-naphthol·S complexes.

Species	Fluorescence lifetime (ns)	Relative Φ_{fl} (%)
1-NpOH, exp.	61 ± 3 [a], 61 ± 2 [b], 60 [c], 60 ± 1 [d]	100
1NpOH·N_2	63 ± 4 [e]	100 ± 7
1NpOH·Ar	45 ± 3	74 ± 5
1NpOH·Kr	6 ± 1	10 ± 2
1NpOH·Xe	2 ± 1	3 ± 1.5

[a] this work

[b] ref. 52

[c] ref. 64

[d] ref. 53

[e] excitation at the 0_0^0 band of isomer A, minor excitation on isomer B

TABLE III. Experimental dissociation energies $D_0(S_0)$ and $D_0(S_1)$ and spectral shifts $\delta\tilde{\nu}$ of the 1-naphthol·S complexes. The true D_0 may lie anywhere within the bracketed interval with equal probability.

Complex	$D_0(S_0)$		$D_0(S_1)$		$\delta\tilde{\nu}$
	cm^{-1}	kJ/mol	cm^{-1}	kJ/mol	cm^{-1}
Ne	<281	<3.36	<283	<3.39	-2
Ar	474±4	5.67±0.05	488±5	5.84±0.06	-14.0
Kr	614±6	7.34 ±0.07	636±6	7.61±0.07	-22.0
Xe	904±24	10.8±0.29	939±24	11.23±0.29	-34.5
N_2 (isomer 1)	565±7	6.676±0.08	579.3±7	6.93±0.08	-14.4
N_2 (isomer 2)	553±18	6.611±0.22	581±18	6.95±0.22	-28.0

TABLE IV. Experimental and calculated dissociation energies $D_0(S_0)$ (in kJ/mol) of the 1-naphthol Face complexes with Ne, Ar, Kr, Xe and N_2 (isomers 1 and 2) and of the corresponding Edge complexes, using the dispersion-corrected DFT methods B97-D3, B3LYP-D3 and ωB97X-D. The calculated changes of vibrational zero-point energy ΔVZPE are given in parentheses. The calculated D_0 that agrees best with experiment is given in bold.

Complex	Experimental	B97-D3	B3LYP-D3	ωB97X-D
		D_0 (ΔVZPE)	D_0 (ΔVZPE)	D_0 (ΔVZPE)
Face				
Ne	< 3.36	2.66 (0.34)	3.13 (0.49)	1.71 (0.29)
Ar	5.67 ± 0.05	**5.40** (0.56)	6.40 (0.61)	4.86 (0.46)
Kr	7.34 ± 0.07	**7.23** (0.57)	8.44 (0.62)	7.65 (0.55)
Xe	10.81 ± 0.28	9.54 (0.70)	**10.42** (0.73)	10.02 (0.69)
N_2 (isomer 1)	6.676 ± 0.08	7.00 (1.84)	7.70 (1.75)	**6.45** (1.68)
N_2 (isomer 2)	6.615 ± 0.22	**6.65** (1.70)	7.36 (1.59)	8.40 (1.75)
Edge				
Ne	-	2.53 (0.64)	2.88	0.50
Ar	-	4.26 (0.65)	4.62	a
Kr	-	4.97 (0.58)	5.33	2.38
Xe	-	5.83 (0.52)	a	a
N_2	-	5.70 (1.89)	6.17	4.24

[a] index-1 saddle point (one imaginary vibrational frequency)

TABLE V. Experimental and calculated dissociation energies $D_0(S_0)$ (in kJ/mol) of the carbazole Face and Edge complexes with Ne, Ar, Kr, Xe and N_2, using the dispersion-corrected DFT methods B97-D3, B3LYP-D3 and ωB97X-D. The calculated zero-point vibrational energy changes ΔVZPE are given in parentheses. The calculated D_0 that agrees best with experiment is given in bold.

Complex	Experimental[a]	B97-D3	B3LYP-D3	ωB97X-D
		D_0 (ΔVZPE)	D_0 (ΔVZPE)	D_0 (ΔVZPE)
Face				
Neon	< 2.56	2.72 (0.39)	3.47 (0.51)	**2.08** (0.08)
Argon	6.35 ± 0.02	**5.70** (0.72)	7.11 (0.74)	4.49 (1.14)
Krypton	8.23 ± 0.058	**8.39** (0.63)	9.33 (0.73)	a
Xenon	10.66 ± 0.02	**10.33** (0.65)	12.77 (0.70)	22.5 (0.88)
N_2	7.503 ± 0.09	7.70 (1.75)	8.56 (1.75)	**7.50** (1.52)
Edge				
Neon	-	$2.58(0.60)$	3.06 (0.69)	0.44 (0.66)
Argon	-	$4.26(0.66)$	4.78 (0.71)	1.49 (0.49)
Krypton	-	$5.57(0.55)$	5.50 (0.63)	2.49 (0.26)
Xenon	-	$5.94(0.45)$	7.38 (0.52)	a
N_2	-	$3.16(1.92)$		

[a] from refs. 32 and 33. The true D_0 may lie anywhere within the bracketed interval with equal probability.

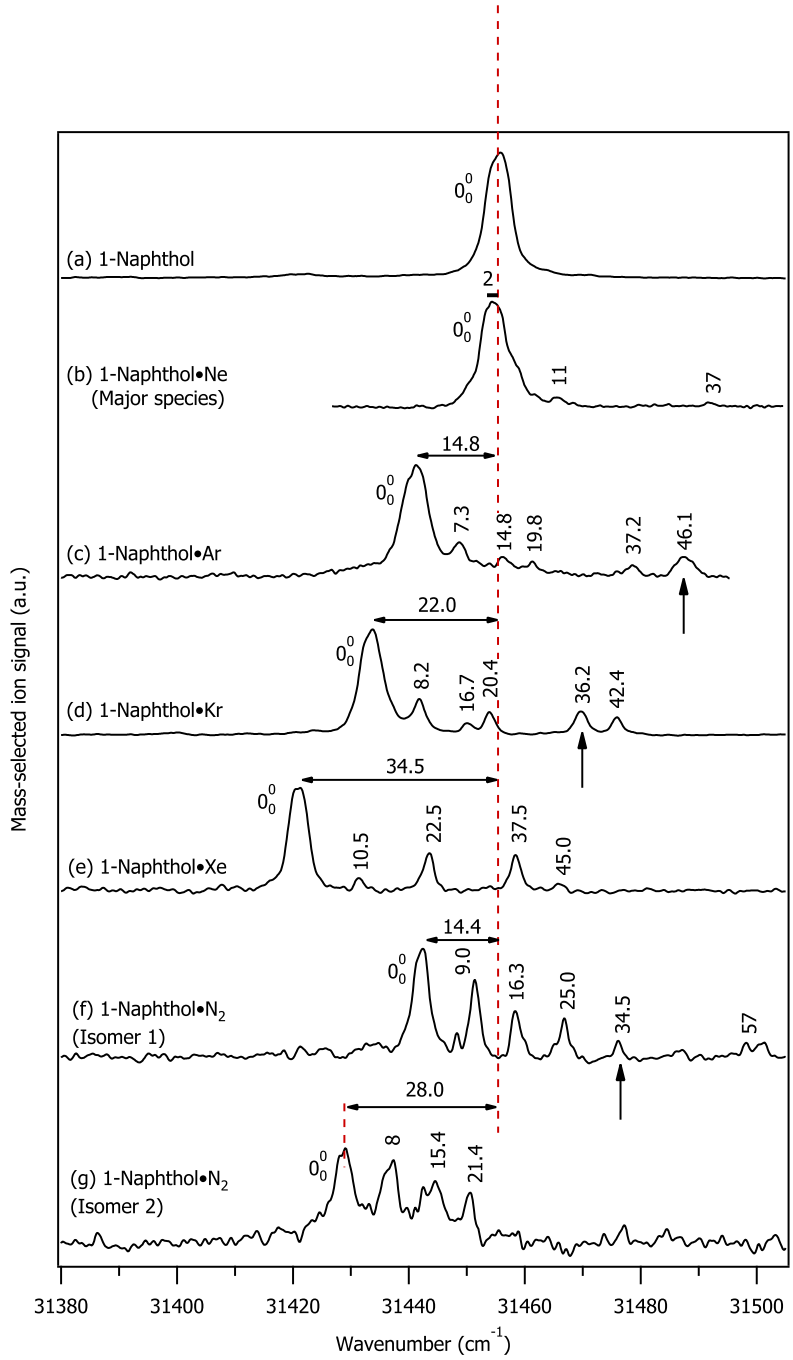

FIG. 1. One-color resonant-two-photon ionization spectra of (a) 1-naphthol and its complexes with (b) Ne, (c) Ar, (d) Kr, (e) Xe, (f,g) two isomers of the N_2 complex that were separated by UV/UV holeburning. The total R2PI and UV-holeburned spectra of the Ne and N_2 complexes are further compared in the supplementary Figures S1 and S2 (SI). The S_1 intermolecular vibronic excitations are labelled with their vibrational energies; assignments are given in Table I. In panels (c,d) and (f), the intermolecular vibronic excitations employed for the D_0 determination are marked with an upward arrow.

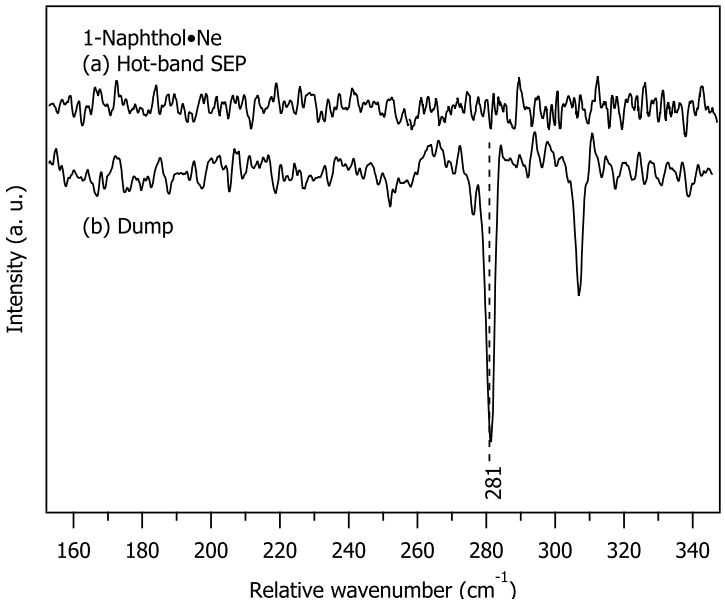

FIG. 2. (a) Hot-band probed SEP-R2PI spectrum and (b) dump laser spectrum of the 1-naphthol·Ne complex. The x-axis is the difference between the pump (0_0^0 band, 31453 cm^{-1}) and dump laser wavenumbers. The lowest-energy vibronic transition in the dump laser spectrum (b) is at 281.4 cm^{-1}; since no corresponding transition is observed in (a), this is the upper limit of the ground-state dissociation energy $D_0(S_0)$.

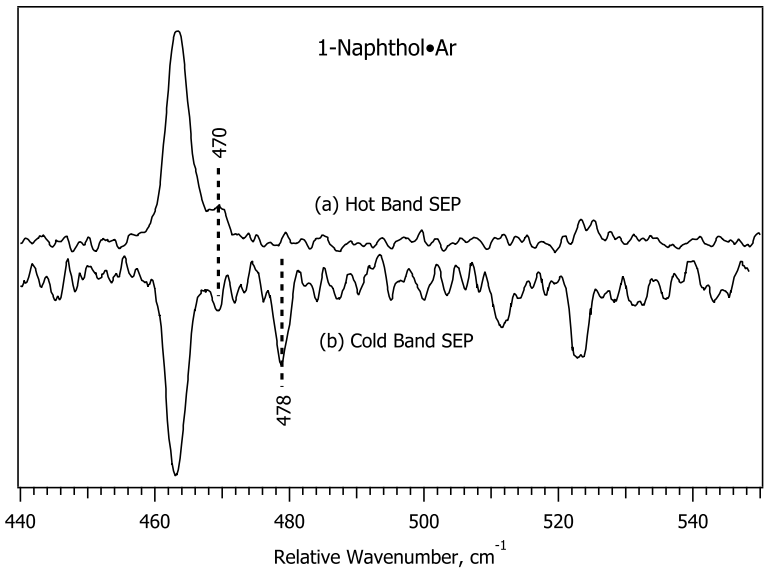

FIG. 3. (a) Hot-band probed and (b) cold-band SEP-R2PI spectra of the 1-naphthol·Ar complex. The $D_0(S_0)$ is bracketed by the highest-energy level at 470 cm^{-1} observed in spectrum (a) and the band at 478 cm^{-1} that appears in the dump spectrum (b), see the dashed lines. The x-axis is the difference between the pump and dump laser wavenumbers.

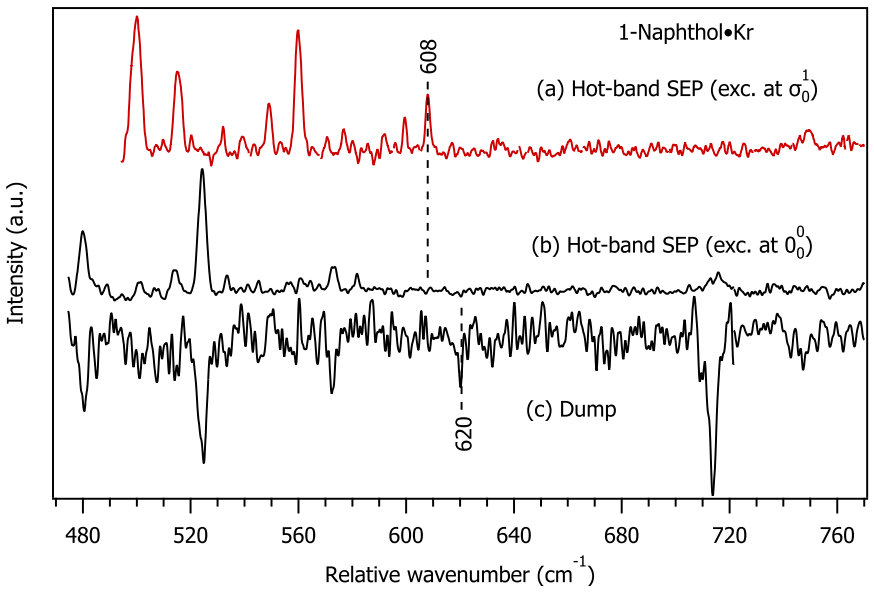

FIG. 4. (a) Hot-band probed SEP-R2PI spectrum with pump excitation at the $0_0^0 + \sigma_0^1$ band at 31423 cm^{-1}, see upward arrow in Figure 1(d). (b) Hot-band probed SEP-R2PI spectrum with pump excitation at the 0_0^0 band, (c) the dump spectrum recorded during the same measurement as spectrum (b). The x-axis is the difference between the pump laser wavenumber [the $0_0^0 + \sigma_0^1$ band for (a), 0_0^0 band for (b,c)] and the dump laser wavenumber. The $D_0(S_0)$ is bracketed by the highest-energy band observed in spectrum (a) at 608 cm^{-1} and the next higher vibronic band observed in the dump spectrum (c) at 620 cm^{-1}.

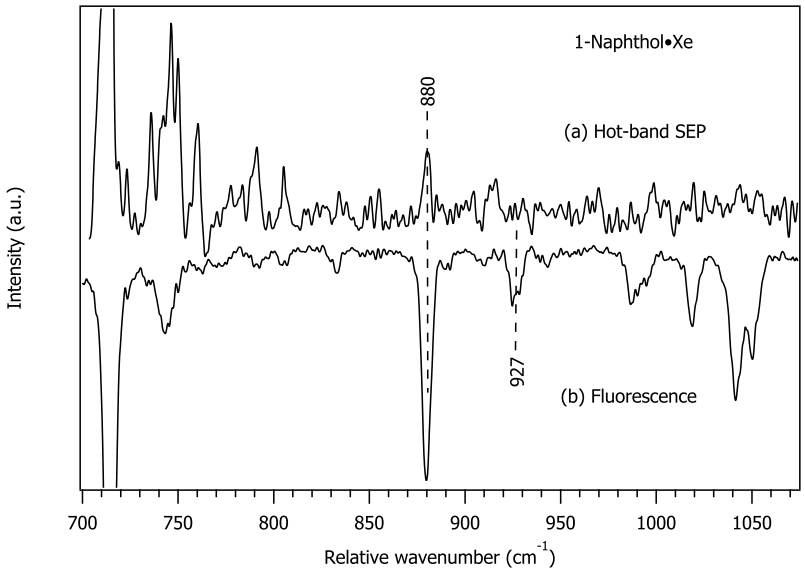

FIG. 5. (a) Hot-band probed SEP-R2PI spectrum and (b) fluorescence spectrum of the 1-naphthol·Xe complex. The x-axis is the wavenumber difference from pump transition (0_0^0 band, 31421 cm^{-1}). The intramolecular vibrational level at 880 cm^{-1} marks the lower limit to the $D_0(S_0)$, the upper limit is given by the 927 cm^{-1} band in the fluorescence spectrum, which is not observed in (a).

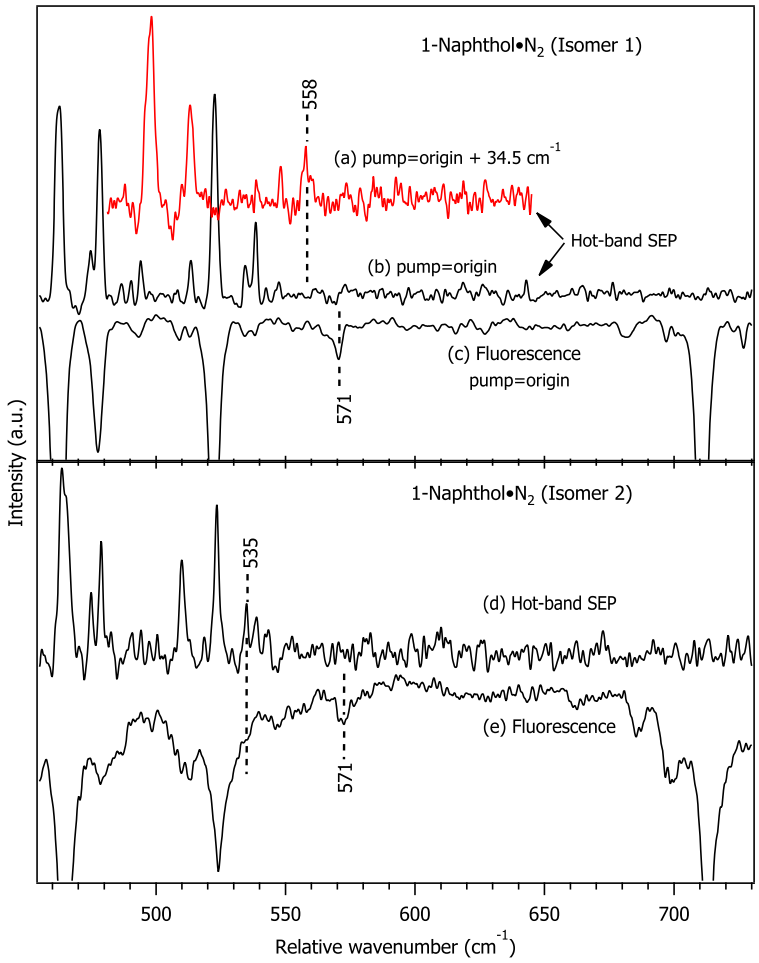

FIG. 6. (a) Hot-band probed SEP-R2PI and dump spectra of isomer 1 of the 1-naphthol·N_2 complex. The x-axis is the difference between the pump (0_0^0, 31440 cm^{-1} for the black spectrum and $0_0^0 + 34.5$, 31474.5 cm^{-1} for the red spectrum) and the dump laser wavenumber. The highest-energy transition at 558 cm^{-1} marks the lower limit to D_0, the fluorescence transition at 571 cm^{-1} marks the upper limit to the $D_0(S_0)$. (b) Hot-band probed SEP-R2PI spectrum and fluorescence spectra of the isomer 2 of the 1-naphthol·N_2 complex. The horizontal axis is the difference between the pump (0_0^0 band, 31428 cm^{-1}) and the dump laser frequency. The highest-energy transition in the SEP spectrum at 535 cm^{-1} marks the lower limit to the $D_0(S_0)$, the band at 571 cm^{-1} in the fluorescence spectrum the upper limit.

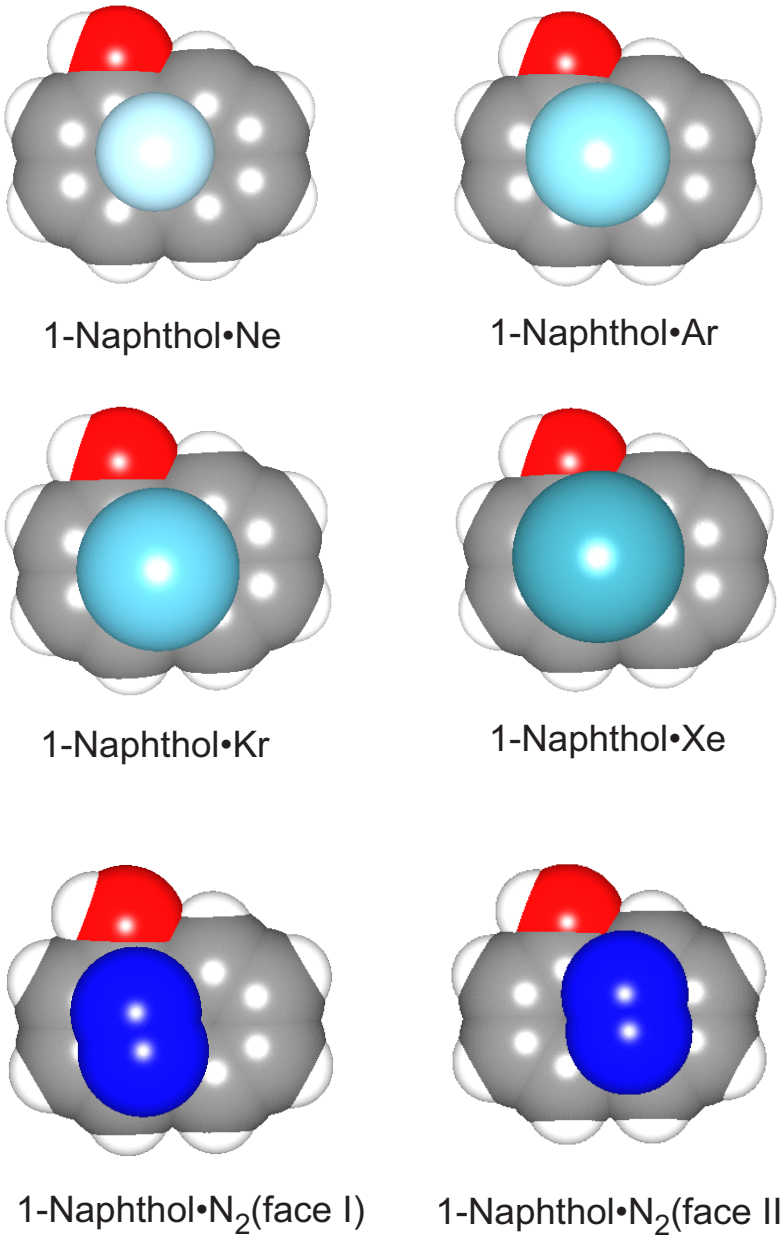

FIG. 7. The B97-D3/def2-TZVPP optimized structures of the complexes of 1-naphthol with (a) Ne, (b) Ar, (c) Kr, (d) Xe, (e) N_2 (isomer 1), (f) N_2 (isomer 2).

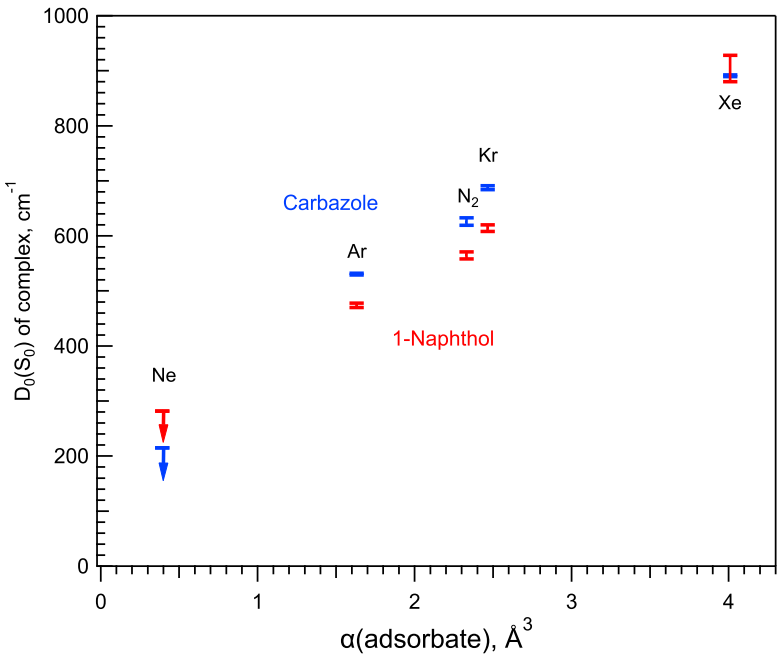

FIG. 8. SEP-R2PI experimental ground-state dissociation energies $D_0(S_0)$ of the carbazole·S (blue) and 1-naphthol·S (red) dispersively bound noble-gas and N_2 complexes, plotted vs. the electronic polarizability α of the adsorbate (in Å^3). For N_2 we plot against $\alpha_{zz} = \alpha_{\|}$, see the text. There are no "bright" vibronic transitions to S_0 state vibrational levels in the vicinity of the dissociation limit of carbazole·Ne and 1-naphthol·Ne, so only upper limits to $D_0(S_0)$ could be measured, indicated by a bar and a downward arrow.

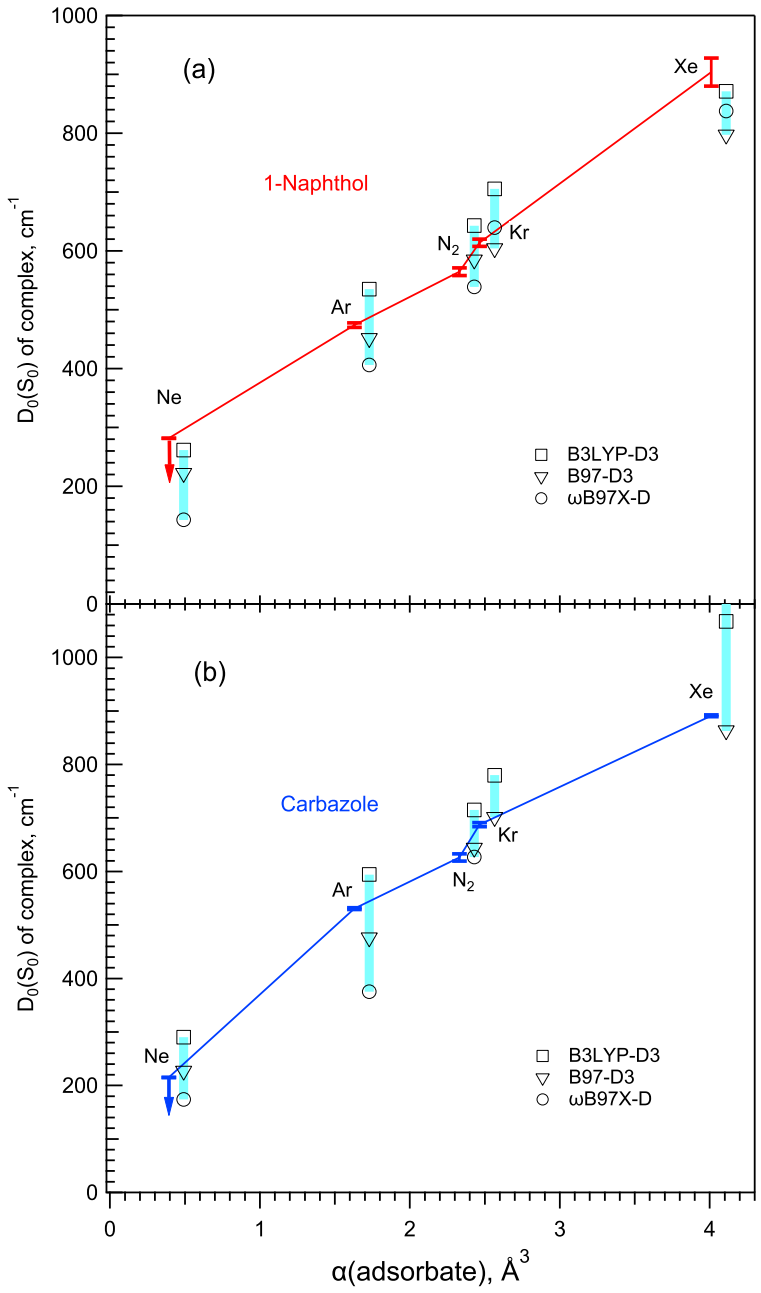

FIG. 9. Comparison of the experimental $D_0(S_0)$ dissociation energies of (a) 1-naphthol·S complexes and (b) the carbazole·S complexes with the B97-D3, B3LYP-D3 and ωB97X-D calculated D_0 values, plotted vs. the electronic polarizability α or $\alpha_{||}$ of the adsorbate (in Å^3). For clarity, the experimental and calculated values are slightly offset in the horizontal direction.

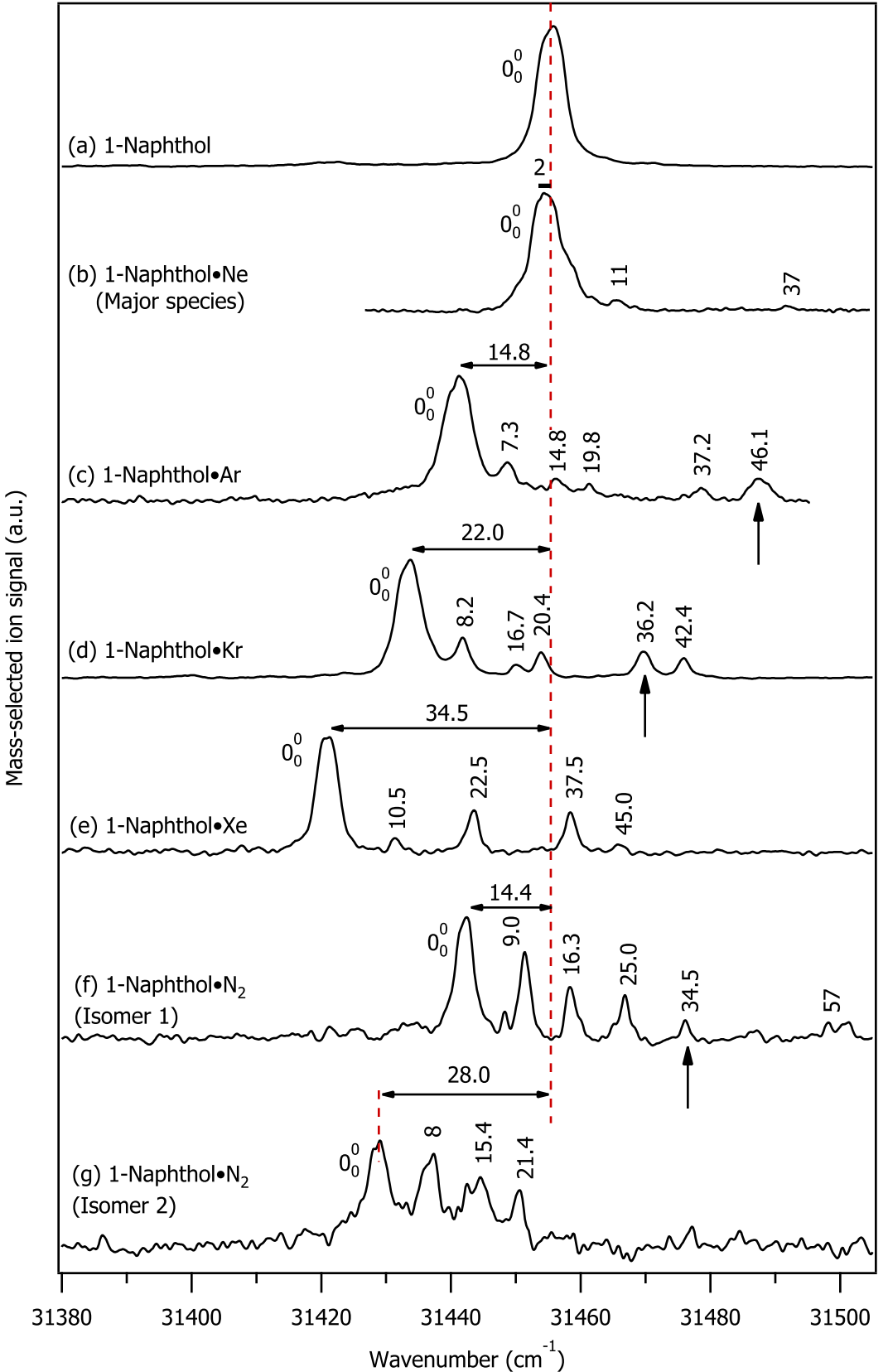
(a) 1-Naphthol
0_0^0
(b) 1-Naphthol•Ne
(Major species)
2
11
37
(c) 1-Naphthol•Ar
14.8
7.3
14.8
19.8
37.2
46.1
(d) 1-Naphthol•Kr
22.0
8.2
16.7
20.4
36.2
42.4
(e) 1-Naphthol•Xe
34.5
10.5
22.5
37.5
45.0
(f) 1-Naphthol•N_2
(Isomer 1)
14.4
9.0
16.3
25.0
34.5
57
(g) 1-Naphthol•N_2
(Isomer 2)
28.0
8
15.4
21.4
Mass-selected ion signal (a.u.)
31380
31400
31420
31440
31460
31480
31500
Wavenumber (cm^{-1})

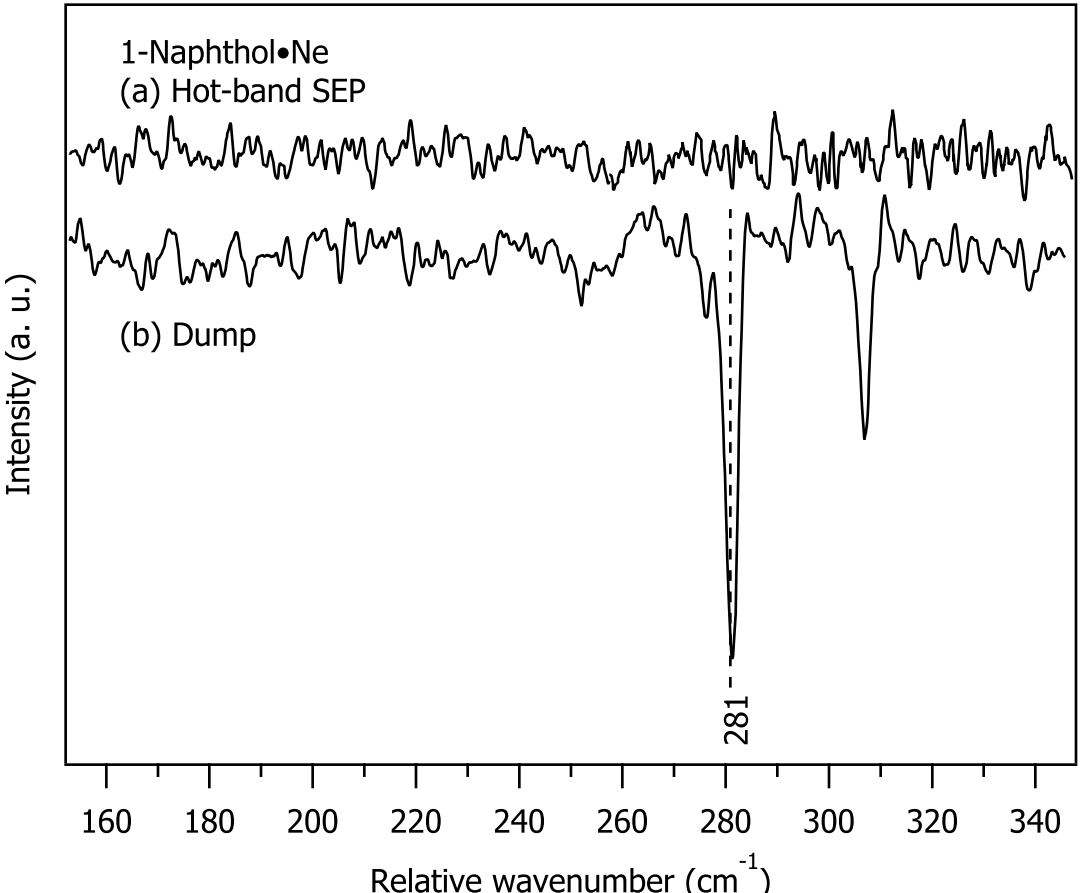
1-Naphthol•Ne
(a) Hot-band SEP
(b) Dump
Intensity (a. u.)
281
160
180
200
220
240
260
280
300
320
340
Relative wavenumber (cm-1)

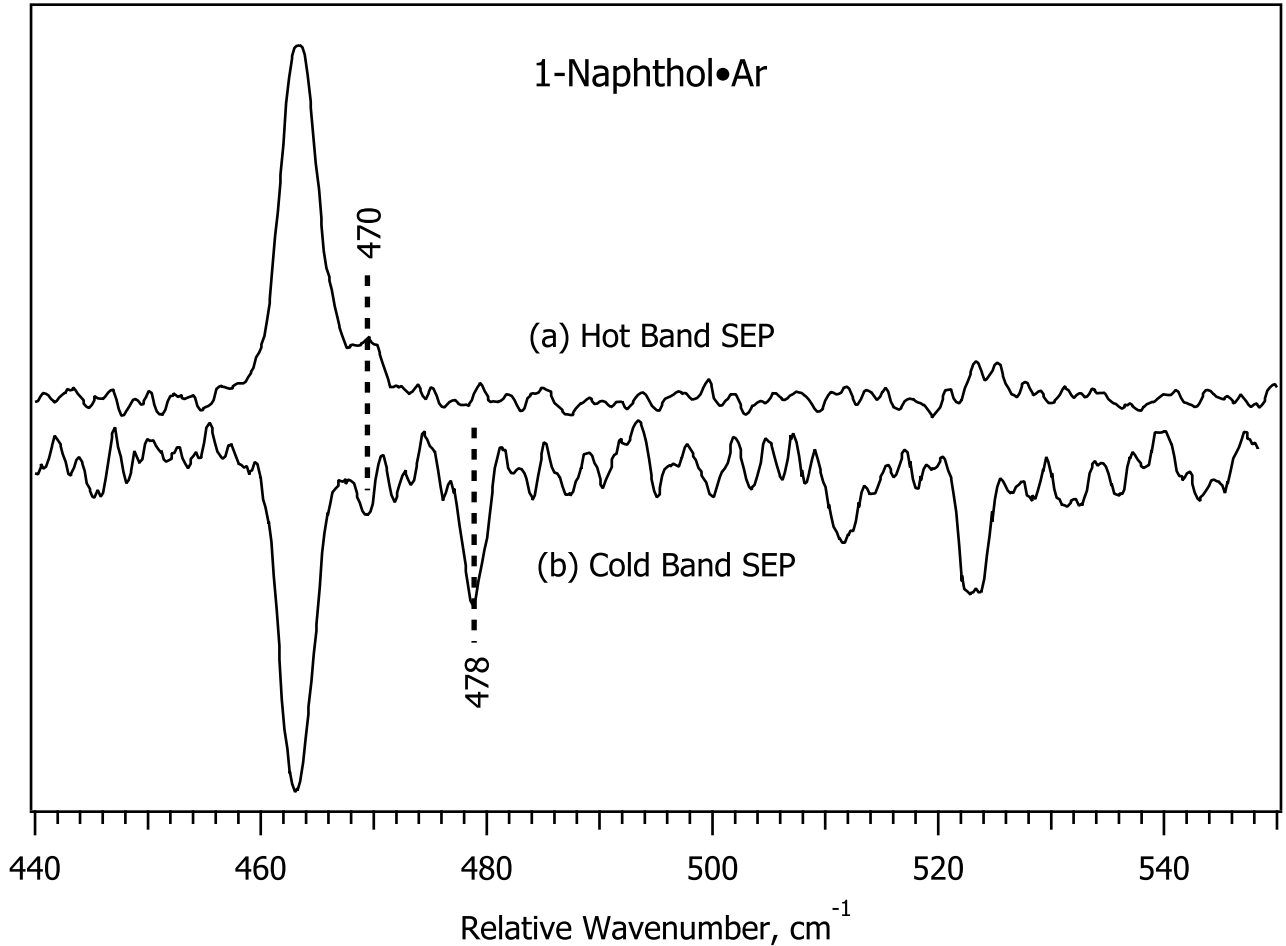
1-Naphthol•Ar
470
(a) Hot Band SEP
(b) Cold Band SEP
478
440
460
480
500
520
540
Relative Wavenumber, cm-1

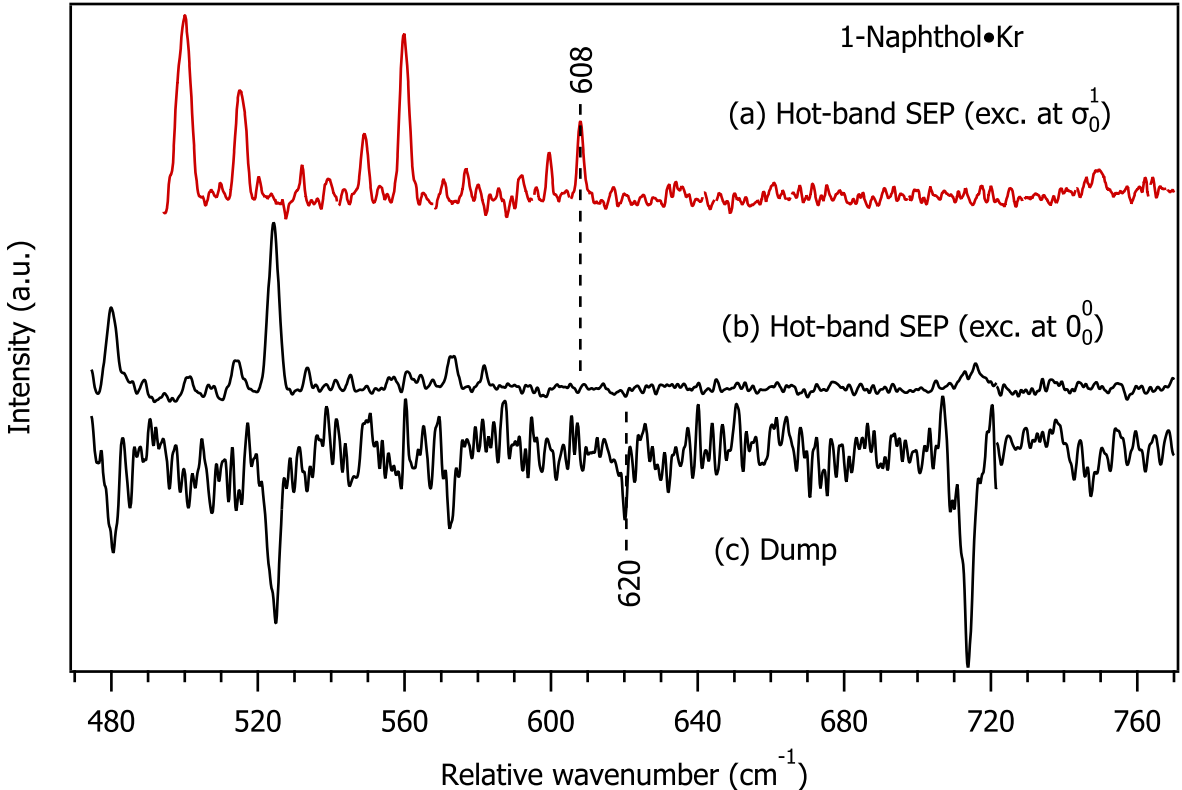
1-Naphthol•Kr
608
(a) Hot-band SEP (exc. at σ_0^1)
(b) Hot-band SEP (exc. at 0_0^0)
620
(c) Dump
Intensity (a.u.)
480
520
560
600
640
680
720
760
Relative wavenumber (cm^{-1})

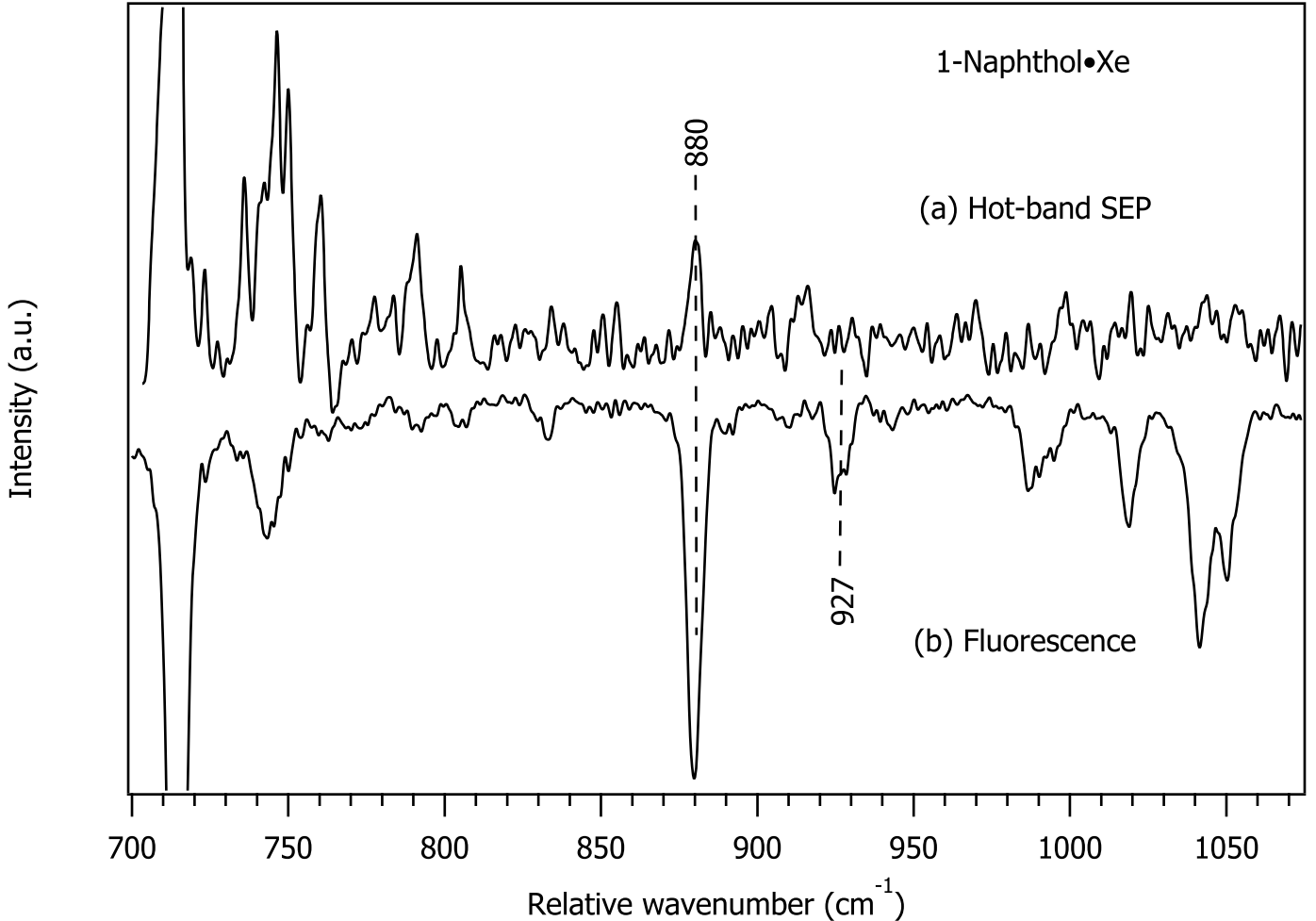
1-Naphthol•Xe
880
(a) Hot-band SEP
927
(b) Fluorescence
Intensity (a.u.)
700
750
800
850
900
950
1000
1050
Relative wavenumber (cm-1)

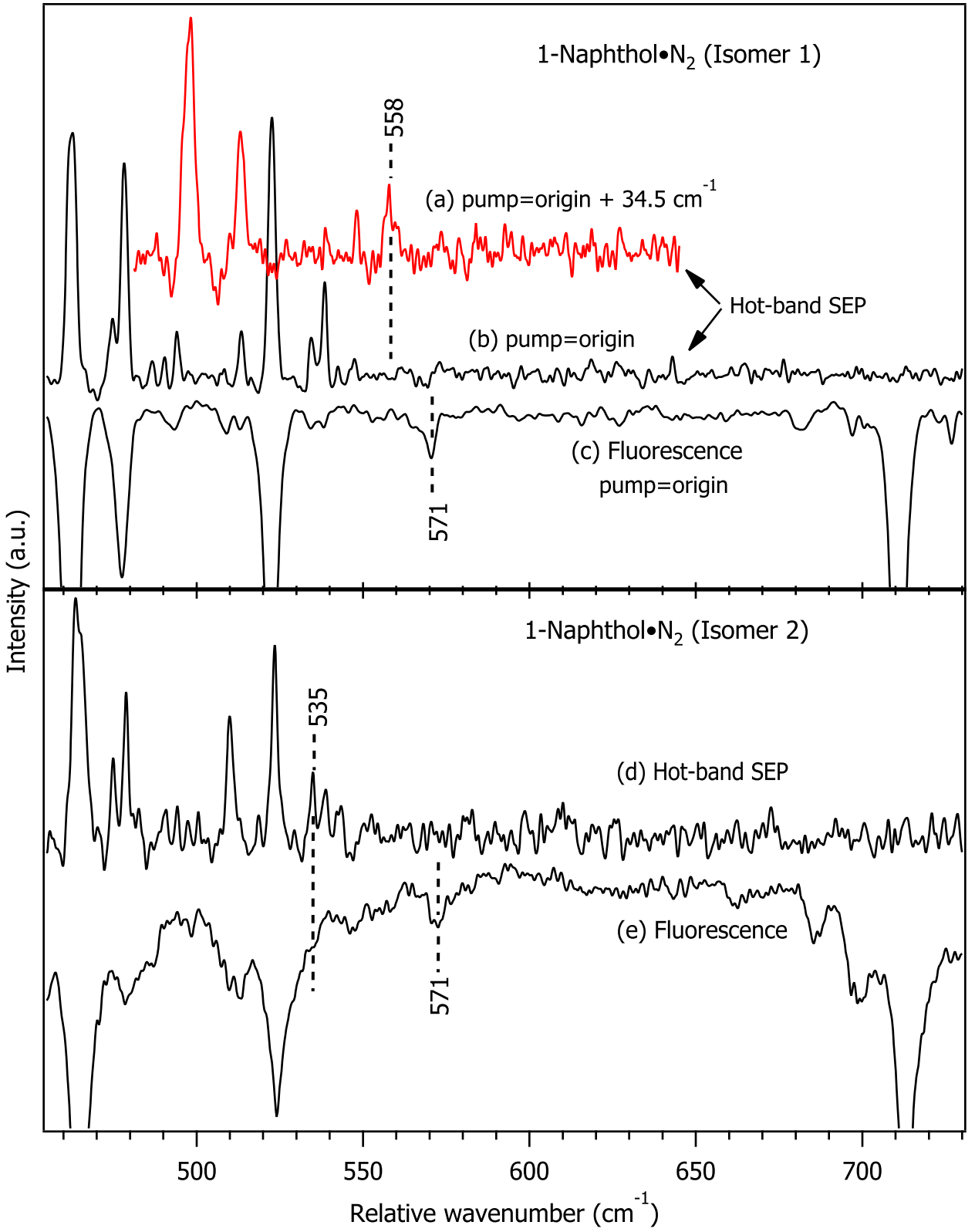
1-Naphthol•N2 (Isomer 1)
558
(a) pump=origin + 34.5 cm-1
Hot-band SEP
(b) pump=origin
(c) Fluorescence
pump=origin
571
1-Naphthol•N2 (Isomer 2)
535
(d) Hot-band SEP
(e) Fluorescence
571
Intensity (a.u.)
500
550
600
650
700
Relative wavenumber (cm-1)

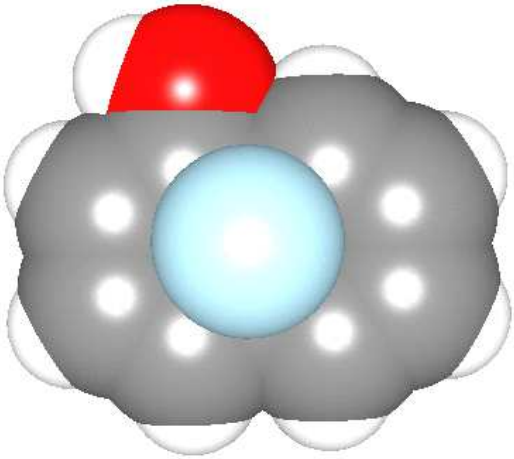

1-Naphthol•Ne

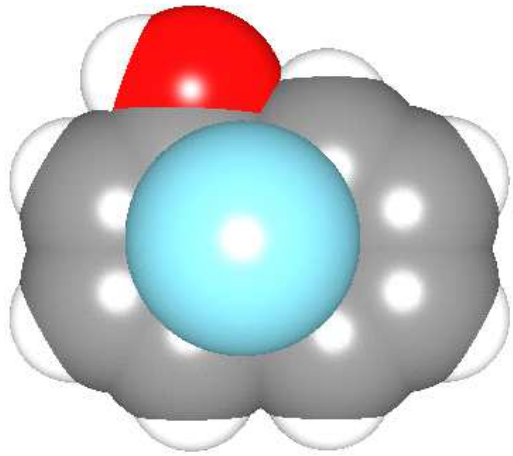

1-Naphthol•Ar

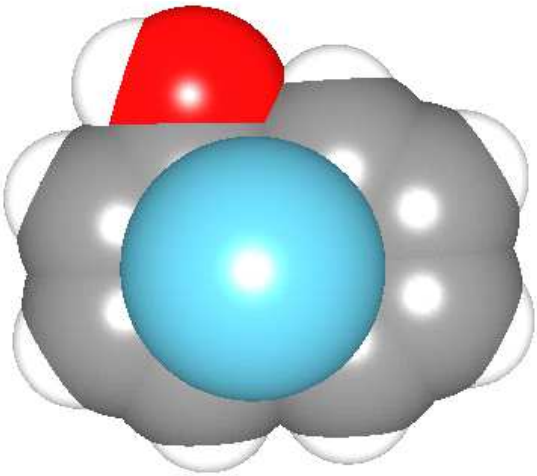

1-Naphthol•Kr

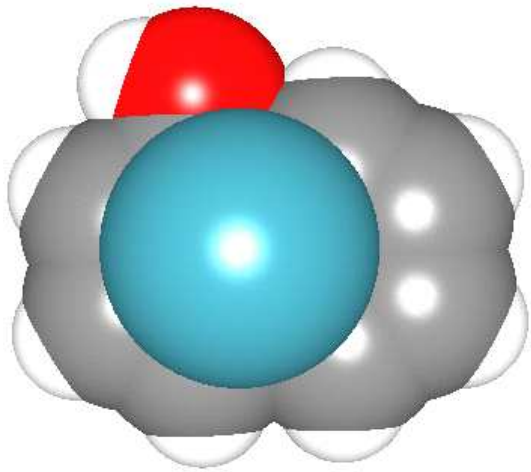

1-Naphthol•Xe

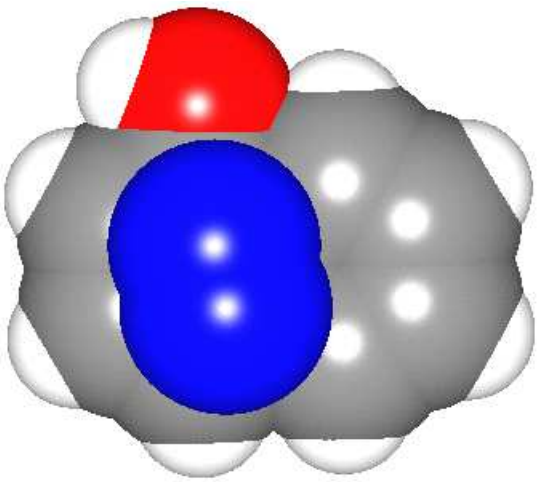

1-Naphthol•N_2(face I)

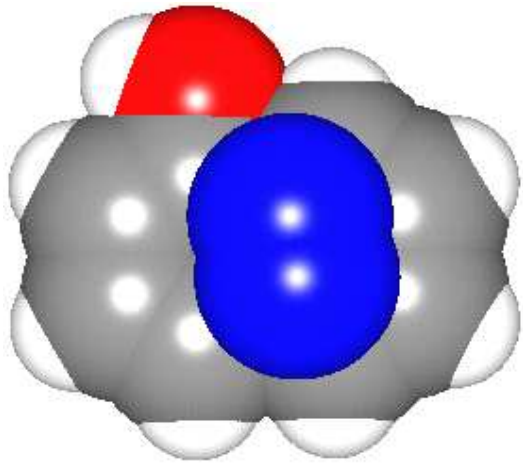

1-Naphthol•N_2(face II)

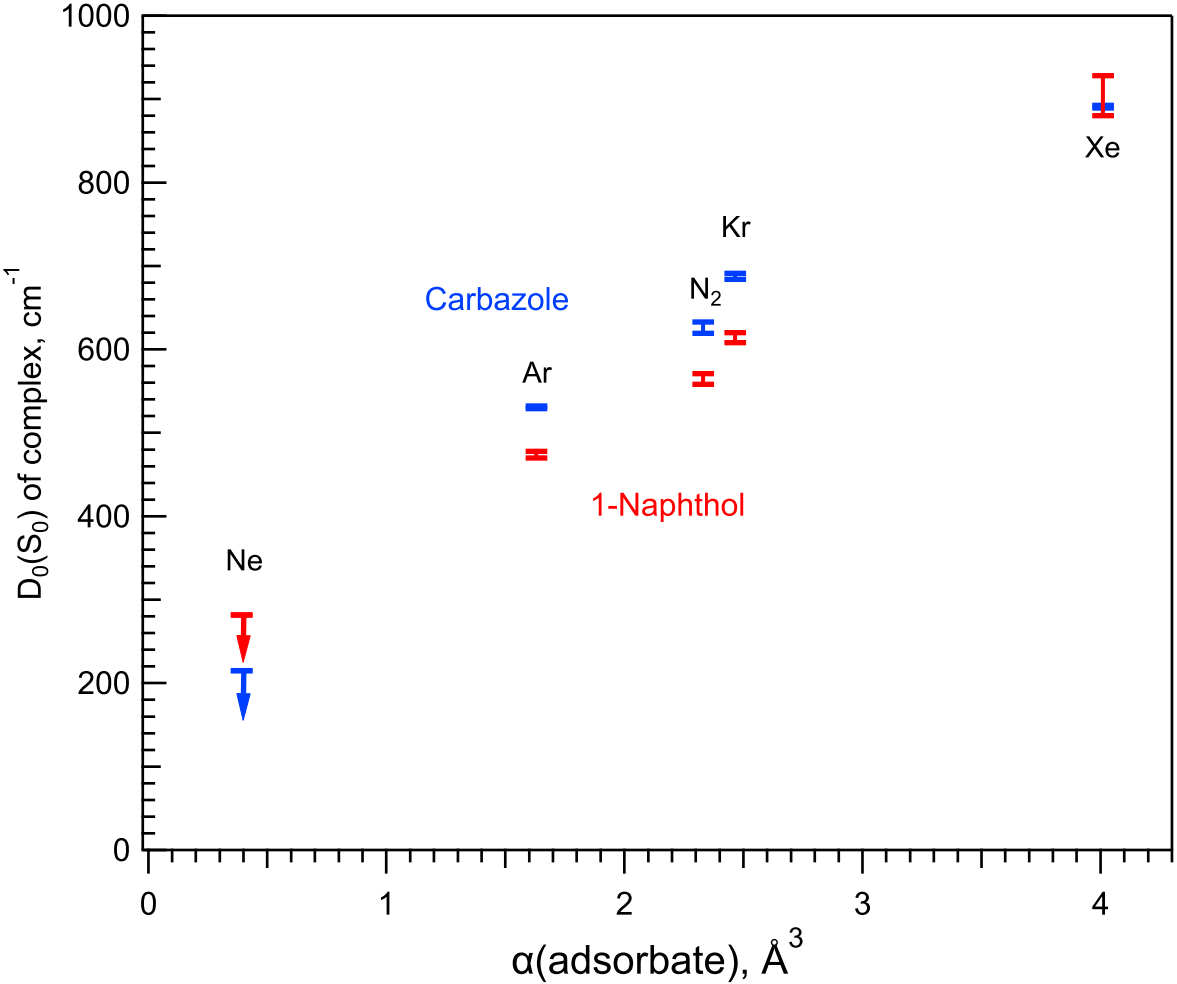
1000
800
600
400
200
0
0
1
2
3
4
$D_0(S_0)$ of complex, cm^{-1}
α(adsorbate), $Å^3$
Carbazole
1-Naphthol
Ne
Ar
N_2
Kr
Xe

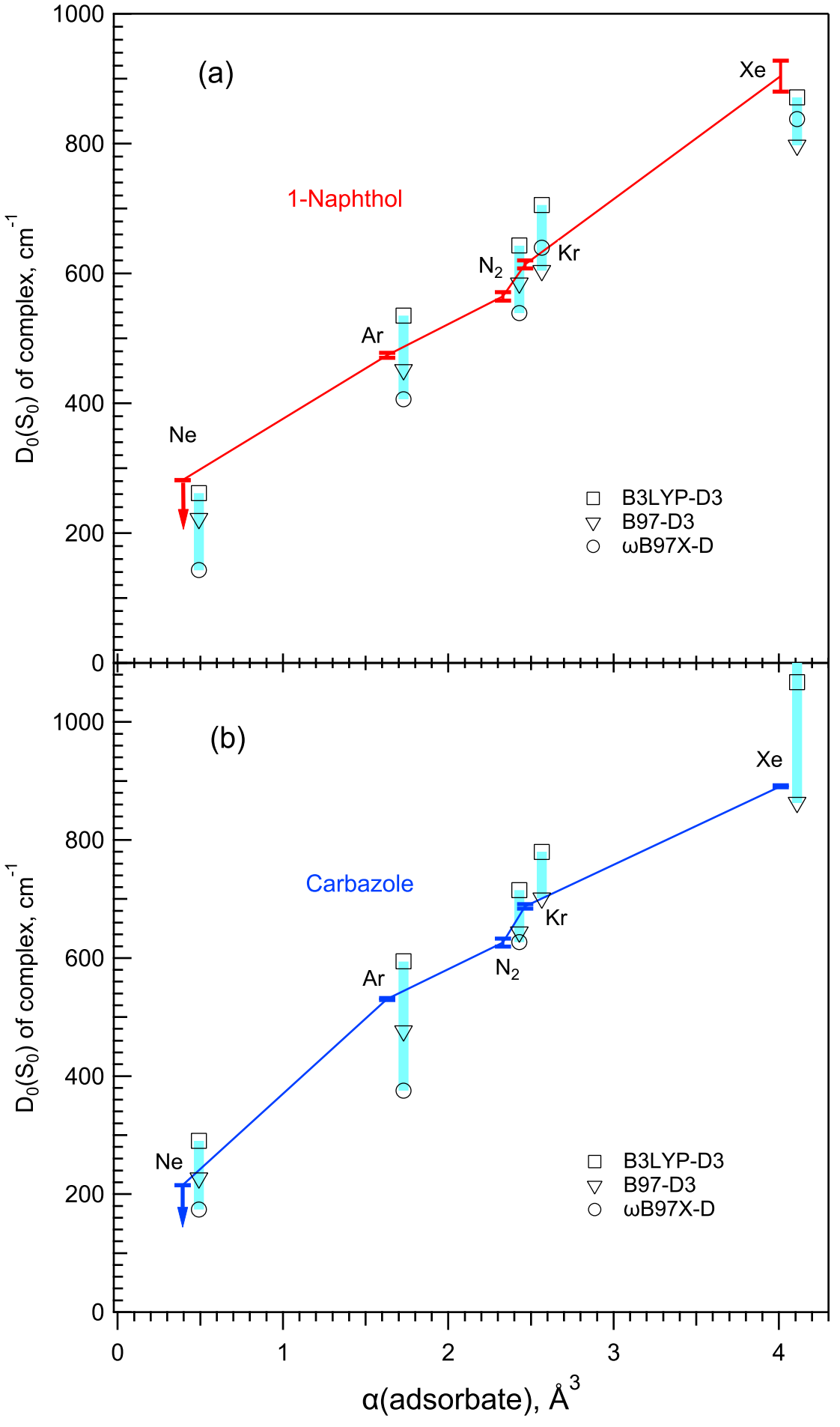
(a)
1-Naphthol
Ne
Ar
N2
Kr
Xe
B3LYP-D3
B97-D3
ωB97X-D
D0(S0) of complex, cm-1
(b)
Carbazole
Ne
Ar
N2
Kr
Xe
B3LYP-D3
B97-D3
ωB97X-D
D0(S0) of complex, cm-1
α(adsorbate), Å3
0
200
400
600
800
1000
0
1
2
3
4